Schweizerische Eidgenossenschaft
Confédération suisse
Confederazione Svizzera
Confederaziun svizra

Federal Department of the Environment, Transport,
Energy and Communications DETEC

Swiss Federal Office of Energy SFOE
Energy Research and Cleantech Division

Deliverable 1 dated 18/11/2021

COSTAM Project

D1.2 – Report on Modular STATCOM structures: Simulations of the selected structures

Date: 18/11/2021

Location: Yverdon-les-Bains

Subsidiser:
Swiss Federal Office of Energy SFOE
Energy Research and Cleantech Section
CH-3003 Bern
www.bfe.admin.ch

Subsidy recipients:
HEIA-FR
Bd. De Pérolles 80, 1700 Fribourg

HEIG-VD
Route de Cheseaux 1, 1401 Yverdon-les-Bains

Authors:
Gislain Grosjean, HEIG-VD, gislain.grosjean@heig-vd.ch
Guillaume Courteau, HEIG-VD, guillaume.courteau@heig-vd.ch
Simon Kissling, HEIG-VD, simon.kissling@heig-vd.ch
Mokhtar Bozorg, HEIG-VD, mokhtar.bozorg@heig-vd.ch
Mauro Carpita, HEIG-VD, Mauro.Carpita@heig-vd.ch

SFOE project coordinators:
Dr. Michael Moser, michael.moser@bfe.admin.ch

SFOE contract number: SI/502069-01

All contents and conclusions are the sole responsibility of the authors

CONTENTS

LIST OF FIGURES

LIST OF TABLES

ABBREVIATIONS

ANPC :	Active Neutral-Point Clamped
BC :	Bridge Cell
BESS :	Battery Energy Storage System
CNPC :	Cascaded Neutral-Point Clamped
CSC :	Current Source Converter
DS :	Double Star
DSCC :	Double Star Chopper-Cells
DVCC:	Dual Vector Current Control
GRD :	Gestionnaire de Réseau de Distribution
FC :	Fix Capacitor
FCI :	Flying Capacitor Inverter
FC-TCR :	Fix Capacitor - Thyristor Controlled Reactor
KCL:	Kirchhoff's Current Law
KVL:	Kirchhoff's Voltage Law
LPF:	Low Pass Filter
MMCC :	Modular Multilevel Cascaded Converter
NNPC :	Nested Neutral-Point Clamped
NPC :	Neutral-Point Clamped
NSCC:	Negative Sequence Current Control
PCC:	Point of Common Coupling
PI:	Proportional Integral
PIR:	Proportional Integral Resonant
PLL:	Phase Locked Loop
PS-PWM:	Phase-Shifted PWM
PSI-LVRT:	Positive Sequence Injection Low-Voltage Ride-Through
PWM :	Pulse Width Modulation
RES :	Renewable Energy Sources
SDBC :	Single Delta Bridge-Cells
SiC :	Silicone Carbite
SM:	SubModule (cell)
SSBC :	Single Star Bridge-Cells
STATCOM :	STAtic synchronous COMpensator
SVG :	Static Var Generator
TCR :	Thyristor Controlled Reactor
THD:	Total Harmonic Distortion
TSC :	Thyristor Switched Capacitor
VSC :	Voltage Source Converter
ZSCC:	Zero Sequence Current Control
ZSVC:	Zero Sequence Voltage Control

1 INTRODUCTION

Different STATCOM topologies are possible to exchange reactive power with the electrical grid. From previous work [1], three configurations have been chosen. They are: SSBC, SDBC and DSCC. These topologies are able to work on medium and high voltage grid and to continue to operate when the grid is unbalanced or when a fault occurs in the grid.

This report presents the detailed analysis of the three selected topologies behaviour with theoretical equations and with simulations done in the Plecs environment. These topologies are assessed for every state of the electrical grid when a fault occurs is taken from the previous analysis in [1].

2 SINGLE STAR BRIDGE-CELLS (SSBC)

The schematic of the SSBC structures is visible on the Figure 2-1. This topology is particularly interesting because it presents the least number of cells, so it makes the solution to be the most practical one in terms of technique, size and cost. On the other side, this structure has no internal circulating current which can give difficulties at zero power exchange.

This system is suitable to exchange a controlled reactive power and to regulate the voltage at the point of common coupling (PCC).

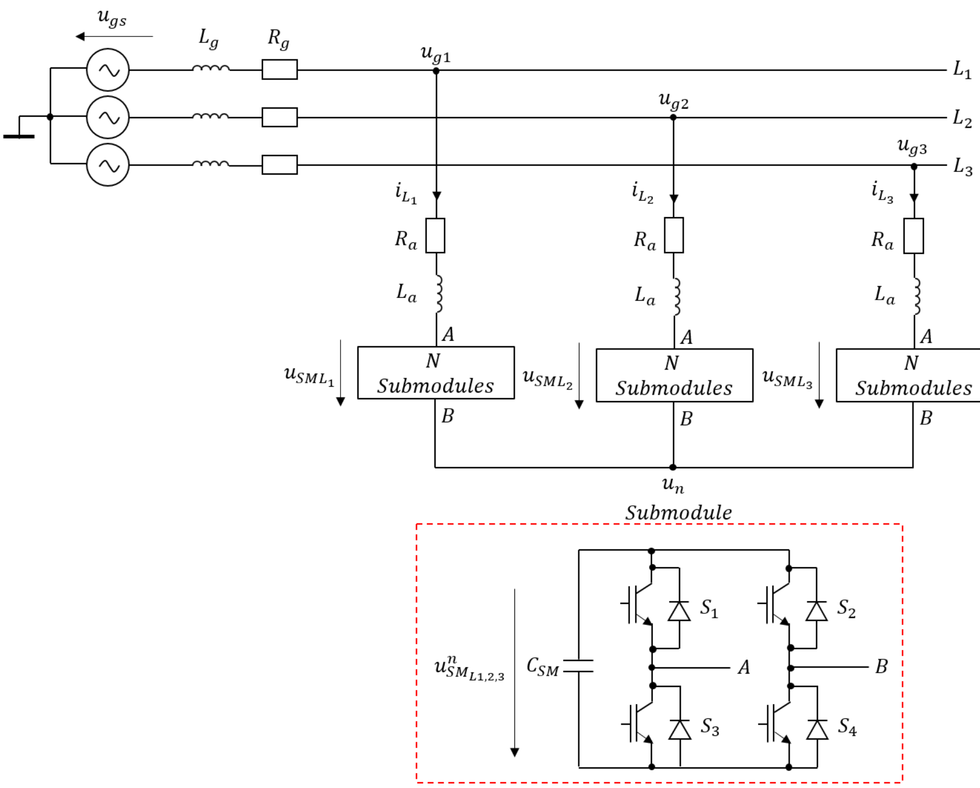

Figure 2-1 : SSBC schematic

To simplify the analysis, the single phase schematic as seen on the Figure 2-2, is used. For that, it is supposed that the grid is balanced.

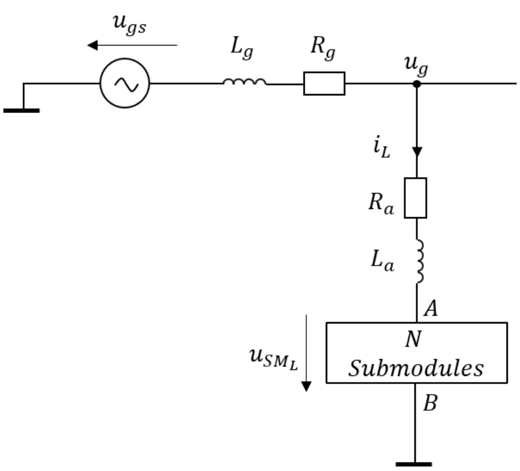

Figure 2-2 : Single phase schematic of the SSBC

2.1 Arm current

From the single phase schematic (Figure 2-2) and the Kirchhoff's laws, the equation (2.1) is extracted.

$$u_g - u_{SM_L} = L_a \cdot \frac{\partial i_L}{\partial t} + R_a \cdot i_L \tag{2.1}$$

From this equation, the transfer function linking the arm current i_L from the voltage produced by the cells u_{SM_L} is visible on the Figure 2-3.

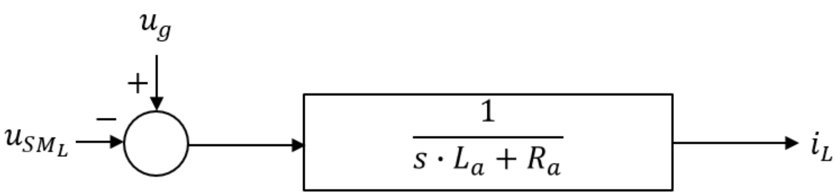

Figure 2-3 : Transfer function of the arm current

2.2 Insertion index and system model

Afterwards, it is necessary to include the insertion index to finalise the system model. The insertion index of the cell n_L^i may take the values -1, 0 or 1. When its value is -1, the capacitor of the cell C_{SM} is inserted to produce a negative voltage. So the power switches are in the states: S_1 & S_4 « *off* » and S_2 & S_3 « *on* » (see Figure 2-4). When its value is 0, the capacitor is not inserted and the outputs A and B are in short circuit. When its value is 1, the capacitor of the cell C_{SM} is inserted to produce a positive voltage. So the power switches are in the states: S_1 & S_4 « *on* » and S_2 & S_3 « *off* ».

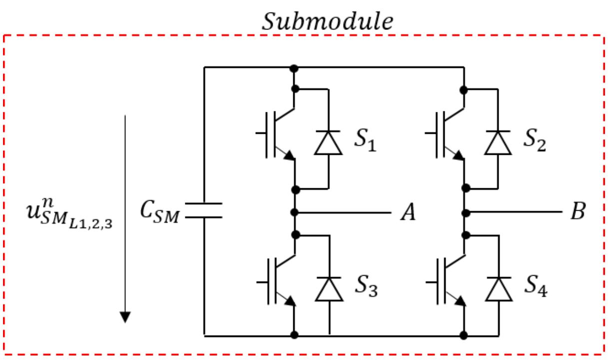

Figure 2-4 : Schematic of a cell

The arm voltage depends of the state of the cells. For the control of the SSBC, it is supposed that it exists a control system which keep the average voltage of each capacitor at the same value. The mathematical description is done in the equation (2.2).

$$u_{SM_L} = \sum_{i=1}^{N} n_L^i \cdot u_{SM_L}^i \cong \sum_{i=1}^{N} n_L^i \cdot \frac{u_{SM_L}^{\Sigma}}{N} = \frac{u_{SM_L}^{\Sigma}}{N} \cdot \sum_{i=1}^{N} n_L^i \tag{2.2}$$

Where $u_{SM_L}^{\Sigma}$ is the sum of each capacitor voltage in a phase and is called the cluster voltage of the phase.

By summing the insertion indices of each cell in an arm divided by the number of cascaded cells as shown in the relation (2.3), the insertion index of each arm is obtained in per unit. The number of possible states is then $2 \cdot N + 1$ discrete values and the value of n_L can vary between -1 and 1. A value of 0 means that all the capacitors are not inserted while a value of ± 1 means that they are all positively or negatively inserted.

$$n_L = \frac{1}{N} \sum_{i=1}^{N} n_L^i \tag{2.3}$$

Inserting the relation (2.3) in (2.2), gives the equation (2.4) to adjust the arm voltage between $\pm u_{SM_L}^{\Sigma}$. The arm voltage depends linearly of the insertion index. Indeed, if N is large or the voltages $u_{SM_L}^i$ are controlled by PWM, n_L can be considered continuous between -1 and 1.

$$u_{SM_L} = n_L \cdot u_{SM_L}^{\Sigma} \tag{2.4}$$

The block diagram of the system model can be completed with the relation (2.4) as presented on the Figure 2-5.

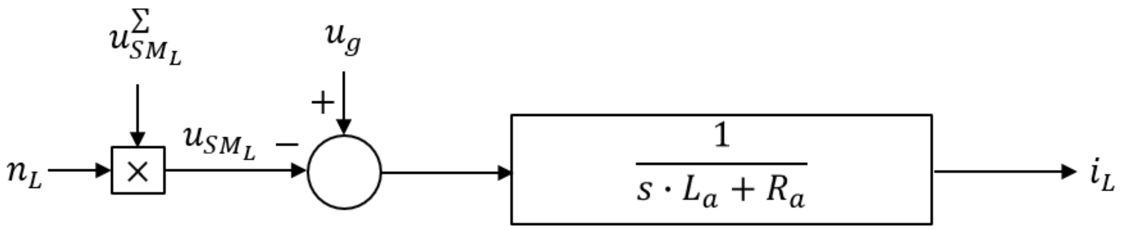

Figure 2-5 : Block diagram completed with the relation (2.4)

According to the relation $i = C \cdot \frac{\partial u}{\partial t}$, the current in the cell is defined by the equation (2.5). The insertion index n_L^i is present. In the case where the capacitor is not inserted, the capacitor does not deliver current.

$$n_L^i \cdot i_L = C_{SM} \cdot \frac{\partial u_{SM_L}^i}{\partial t} \quad with\ i = 1,2,\dots,N \tag{2.5}$$

As the SSBC is composed of several cascaded cells, the current i_L depends on the number of active cells. The result gives the equation (2.6).

$$C_{SM} \cdot \sum_{i=1}^{N} \frac{\partial u_{SM_L}^i}{\partial t} = i_L \cdot \sum_{i=1}^{N} n_L^i \tag{2.6}$$

Using the arm insertion index equation (2.3), the relationship (2.6) simplifies to equation (2.7). The factor N is derived from the fact that the insertion index n_L is in per unit.

$$\boxed{(2.3)\ \&\ (2.6)} \Rightarrow C_{SM} \cdot \sum_{i=1}^{N} \frac{\partial u_{SM_L}^{i}}{\partial t} = i_L \cdot N \cdot n_L \tag{2.7}$$

Supposing that the average voltage of each cell are the same, the equation (2.7) can be simplified to the relation (2.8).

$$\frac{C_{SM}}{N} \cdot \frac{\partial u_{SM_L}^{\Sigma}}{\partial t} = i_L \cdot n_L \tag{2.8}$$

Finally, using the relation (2.8), it is possible to establish the block diagram of the whole system model as shown in Figure 2-6.

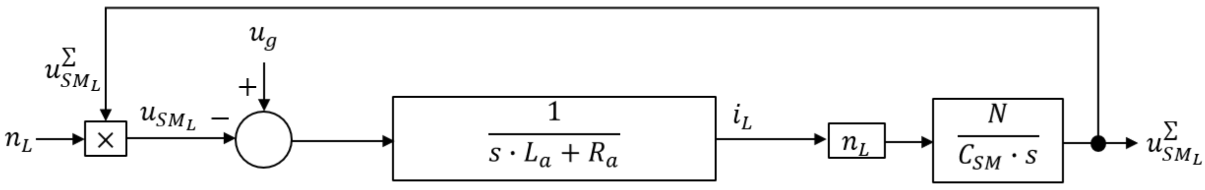

Figure 2-6 : Block diagram of the SSBC system model

2.3 Control of the system

This chapter explains the development required to implement a control strategy of the SSBC. The goal is to control the exchange of reactive power between the system and the grid. The reference of the control is $\mathrm{Q_{AC}}$.

From the Figure 2-6 which represents the system model to control, it can be seen that the input variable of the system is the insertion index n_L. This variable has a double impact on the control. It acts on the generation of the arm voltage u_{SM_L} by multiplying the cluster voltage $u_{SM_L}^{\Sigma}$ but also in the variation of this cluster voltage. The control of the system with the insertion index n_L is therefore non-linear and complex to handle.

In order to avoid this problem of non-linearity, it is possible to define the important quantities to be adjusted. These quantities are:

- i_L : the arm current which acts in the reactive power control and the variation of $u_{SM_L}^{\Sigma}$.
- $u_{SM_L}^{\Sigma}$: the cluster voltage which undergoes variations depending on i_L and permits to generate the voltage u_{SM_L} for the control of the system (thus of i_L).

The quantities i_L and $u_{SM_L}^{\Sigma}$ represent the internal dynamic state of the system. Thus, it seems obvious that the voltage $u_{SM_L}^{\Sigma}$ will be control using the arm current i_L. So, there is only one current to adjust, the arm current i_L.

According to the relation (2.1), the current i_L is easily controlled with the arm voltage u_{SM_L}. However, the system model has the insertion index n_L as input. Therefore, the relation (2.4), which links the voltage to the insertion index, is used. Assuming that the delay of the voltage control is negligible compared to the average model of the SSBC, it is then possible to replace the voltage by its reference value $u_{SM_L}^{*}$, which gives the equation (2.9).

$$n_L = \frac{u_{SM_L}}{u_{SM_L}^{\Sigma}} \cong \frac{u_{SM_L}^{*}}{u_{SM_L}^{\Sigma}} \tag{2.9}$$

From this last relationship, the control scheme shown on the Figure 2-7 can be used to define the insertion index as a function of the arm voltage.

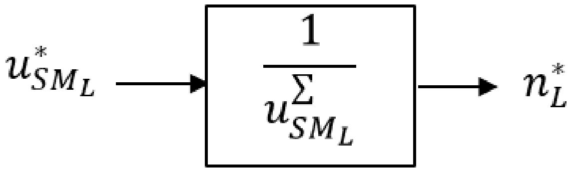

Figure 2-7 : Control scheme of the voltage

It is obvious that this control scheme is simply the inverse of the input stage of the system model which was shown at the Figure 2-6.

2.4 Current control

The arm current regulator ($G_{Ri_L}(s)$) generates the arm voltage u_{SM_L}. The Figure 2-8 shows how this regulator is integrated in the control scheme.

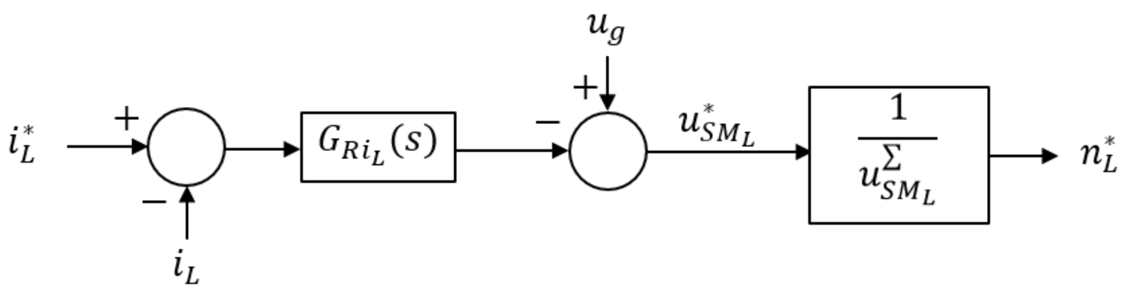

Figure 2-8 : Scheme control of the current

There are 2 important points to note in the above image:

- The voltage u_g is summed in order to perform a voltage feed-forward to counteract the grid voltage.
- The output of the arm current regulator is inverted to take in count the negative sign on the arm voltage in the system model to control (see Figure 2-6).

Until now, a single-phase system was always considered. Now it is possible to switch to a three-phase system. To do this, taking the single-phase model, the arms current are handled with the space vectors. It is assumed that a PLL (Phase Locked Loop) gives the phase θ of the grid and is used to do the Park and Park inverse transformations to obtain the dq/three-phase values. The result is shown in Figure 2-9. Note that the insertion index $\overrightarrow{n^*_L}$ is obtained by dividing the reference voltages $\overrightarrow{u^*_{SM_{Li}}}$ by the average value of the cluster voltage for each phase, i.e., $3/\left(\sum_{i=1}^{3} u^\Sigma_{SM_{Li}}\right)$. This is because the three-phase system is assumed to be balanced and thus the voltages $u^\Sigma_{SM_{Li}}$ are equal.

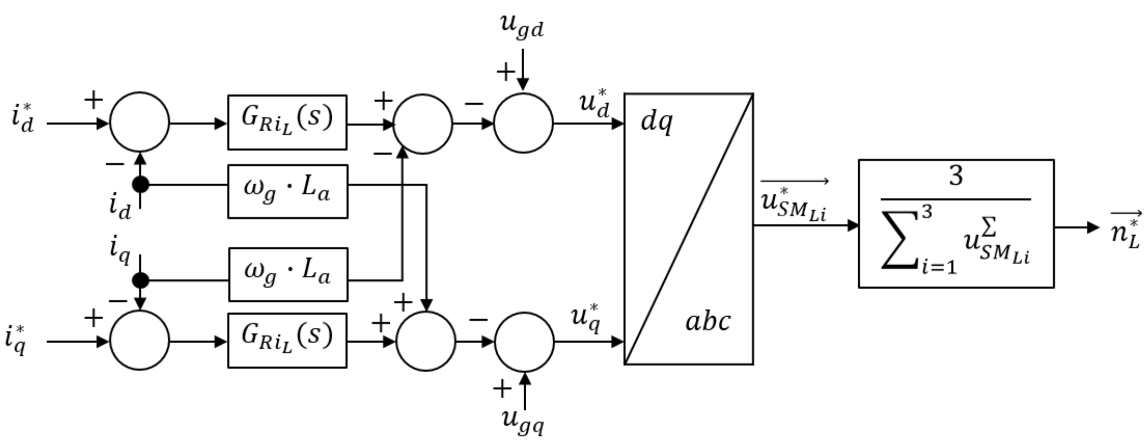

Figure 2-9 : Scheme control of the three-phase currents

2.5 Voltage control

In section 2.3, it was explain that the sum of the arm capacitor voltages $u_{SM_L}^{\Sigma}$ represents the internal dynamic state of the system. If the control scheme in Figure 2-9 is used, the voltages $u_{SM_L}^{\Sigma}$ will diverge and reach the physical limits of the different electronic components. Therefore, these voltages must be controlled.

By injecting equation (2.4) into equation (2.8), the relation (2.10) is obtained.

$$\boxed{(2.4)\ \&\ (2.8)} \Rightarrow u_{SM_L}^{\Sigma} \cdot \frac{C_{SM}}{N} \cdot \frac{\partial u_{SM_L}^{\Sigma}}{\partial t} = i_L \cdot u_{SM_L} \tag{2.10}$$

The mathematical relation (2.11) can then be used to modify the relation (2.10).

$$u_{SM_L}^{\Sigma} \cdot \frac{\partial u_{SM_L}^{\Sigma}}{\partial t} = \frac{1}{2} \cdot \frac{\partial \left(u_{SM_L}^{\Sigma}\right)^2}{\partial t} \tag{2.11}$$

This gives the equation (2.12).

$$\boxed{(2.10)\ \&\ (2.11)} \Rightarrow \frac{C_{SM}}{2 \cdot N} \cdot \frac{\partial \left(u_{SM_L}^{\Sigma}\right)^2}{\partial t} = i_L \cdot u_{SM_L} \tag{2.12}$$

The energy in a capacitor is obtained by the equation (2.13).

$$E = \frac{1}{2} \cdot C \cdot u^2 \Rightarrow \frac{\partial E}{\partial t} = \frac{1}{2} \cdot C \cdot \frac{\partial (u)^2}{\partial t} \tag{2.13}$$

Thus, from equation (2.12) , it is possible to obtain the equation (2.14).

$$\boxed{(2.12)\ \&\ (2.13)} \Rightarrow \frac{\partial E_L}{\partial t} = i_L \cdot u_{SM_L} \tag{2.14}$$

The arm voltage and current are desired purely sinusoidal, so they are described in the equations (2.15) and (2.16).

$$u_{SM_L} = \hat{U}_{SM_L} \cdot \cos(\omega_g \cdot t) \tag{2.15}$$

$$i_L = \hat{I}_L \cdot \cos(\omega_g \cdot t - \varphi) \tag{2.16}$$

Injecting relations (2.15) and (2.16) into (2.14), equation (2.17) is established.

$$\boxed{(2.14), (2.15)\ \&\ (2.16)} \Rightarrow \frac{\partial E_L}{\partial t} = \hat{U}_{SM_L} \cdot \hat{I}_L \cdot \cos\left(\omega_g \cdot t\right) \cdot \cos\left(\omega_g \cdot t - \varphi\right) \tag{2.17}$$

It is then possible to simplify the relation (2.17) by applying a trigonometric relation to obtain the equation (2.18). Then the single-phase AC power from the relation $P = U \cdot I \cdot \cos(\varphi)$ comes.

$$\frac{\partial E_L}{\partial t} = \overbrace{\boxed{\frac{\hat{U}_{SM_L} \cdot \hat{I}_L}{2} \cdot \cos(\varphi)}}^{P_{mono_{AC}}} + \frac{\hat{U}_{SM_L} \cdot \hat{I}_L}{2} \cdot \cos(2 \cdot \omega_g \cdot t - \varphi) \tag{2.18}$$

The time-dependent term in this last equation has no influence on the derivative of the energy average. This means that it is the active power that allows the adjustment of the internal energy of the system as shown in relation (2.19).

$$\frac{\partial \bar{E}_L}{\partial t} = \overbrace{\boxed{\frac{\hat{U}_{SM_L} \cdot \hat{I}_L}{2} \cdot \cos(\varphi)}}^{P_{mono_{AC}}} \tag{2.19}$$

By integrating equation (2.19), the relation (2.20) is obtained. The arm energy is decomposed into constant term $\bar{E}_L$ which is the average value and a time-dependent term ΔE_L which represents the ripple in the energy arm. It is interesting to note that the frequency of the ripple is twice that of the grid.

$$E_L = \bar{E}_L + \overbrace{\boxed{\frac{\hat{U}_L \cdot \hat{I}_L}{4 \cdot \omega_g} \cdot \sin(2 \cdot \omega_g \cdot t - \varphi)}}^{\Delta E_L} \tag{2.20}$$

Since the goal is to have the cluster voltage equal to the reference cluster voltage ($u_{SM_L}^{\Sigma} = u_{SM_L}^{\Sigma *}$), this gives the relation (2.21). This relation defines the average reference value of the arm energy.

$$\bar{E}_L^* = \frac{1}{2} \cdot \frac{C_{SM}}{N} \cdot \left(u_{SM_L}^{\Sigma *}\right)^2 \tag{2.21}$$

As seen previously, to increase the energy, it is necessary to increase the active power. Since the three-phase system is assumed to be balanced (and it must be for its proper operation), the energy in the 3 phases can be increased by using the three-phase active power and therefore by increasing the reference current i_d^*. To do this, it is possible to implement a PI energy controller that respects the control law (2.22).

$$i_d^* = K_{pE} \cdot (\bar{E}_L^* - \bar{E}_L) + K_{iE} \cdot \frac{1}{s} \cdot (\bar{E}_L^* - \bar{E}_L) \tag{2.22}$$

To measure the average value of energy, it is necessary to add a low-pass filter “LFP” which leads to the relationship (2.23).

$$\begin{gathered} i_d^* = K_{pE} \cdot (\bar{E}_L^* - LPF\{E_L\}) + K_{iE} \cdot \frac{1}{s} \cdot (\bar{E}_L^* - LPF\{E_L\}) \\ With : \bar{E}_L^* = \frac{1}{2} \cdot \frac{C_{SM}}{N} \cdot \left(u_{SM_L}^{\Sigma *}\right)^2 \end{gathered} \tag{2.23}$$

The cutoff frequency of the filter can be set to 1/10 of the ripple frequency i.e., $\frac{\omega_g}{5}$.

Finally, the complete control scheme of the SSBC is shown in Figure 2-10. To simplify the control scheme, the PLL, Park and Park inverse transformation are not shown.

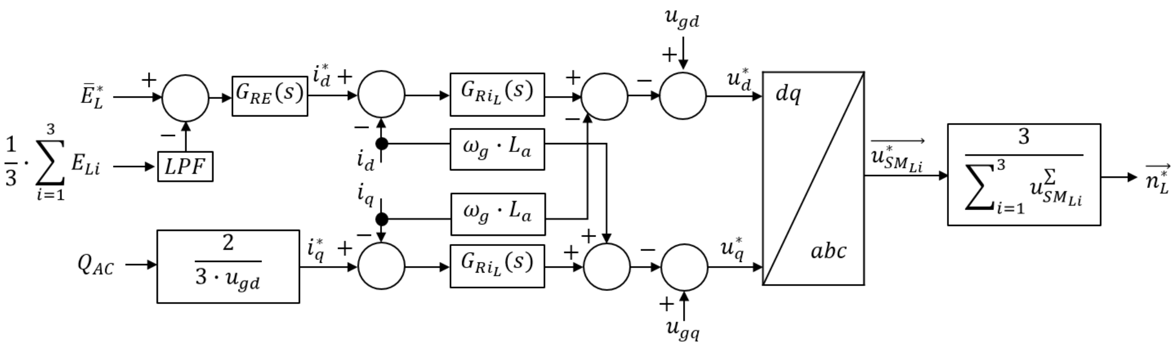

Figure 2-10 : Complete control scheme of the SSBC in a balanced grid

2.6 UNBALANCED GRID

In this project, the STATCOM has to continue to operate properly even if the grid is unbalanced or if a fault occurs in the grid. When the system operates in unbalanced conditions, it is important to use the method of symmetrical components [2]. This method is also explained in [3] and [4]. In brief, this method shows that an unbalanced poly-phase system may be decomposed in three balanced poly-phase sequences. The positive, negative and zero sequences. In reverse order, the sum of these three balanced poly-phase sequences gives the unbalanced poly-phase system of the beginning. Note that the negative sequence turns the opposite way than the positive sequence.

The transformation which permits to pass from the unbalanced system to the three balanced poly-phase sequences is called the Fortescue transformation and works in the phasors domain. In [3], and [5] for more details, an extension of the work of Fortescue to apply the method of the symmetrical components in the time domain is done. This extended method is called the Lyon transformation and will be used in this project.

The Figure 2-11 represents the control scheme of the SSBC when it is used in an unbalanced grid. The PLL block allows to do the synchronization between the grid voltages and the control. The Lyon blocks give the positive and negative sequence of the grid voltage and current. The Park transformations permit to obtain the dq phasors for the positive and negative sequences.

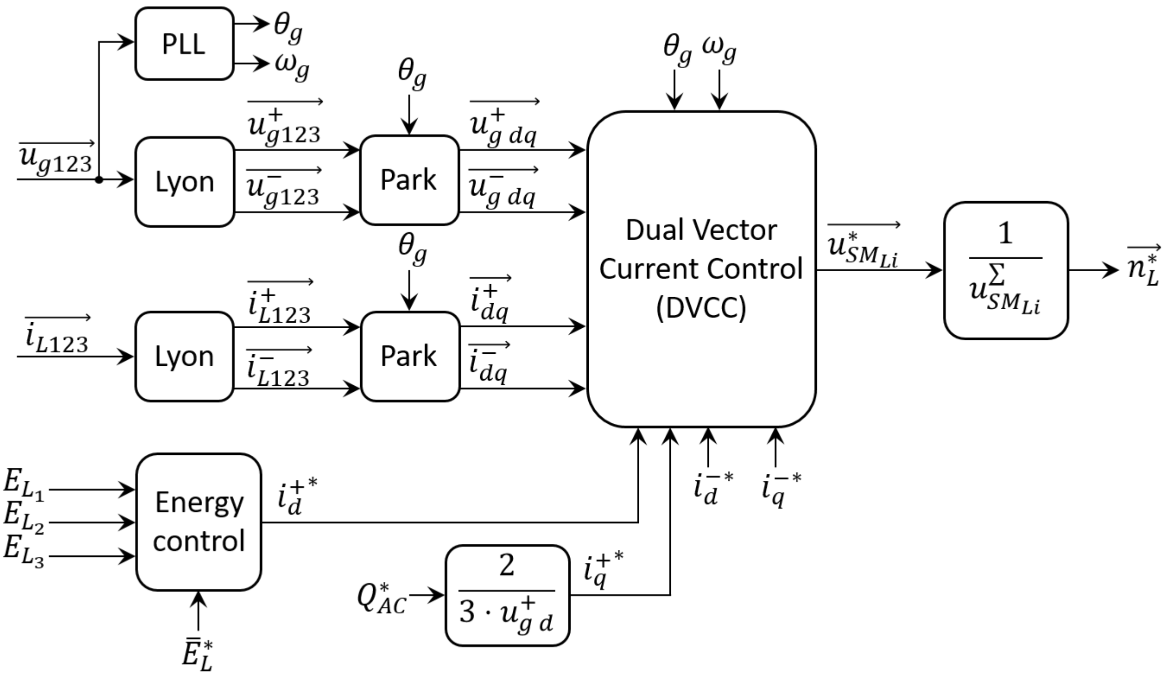

Figure 2-11 : Control scheme of the SSBC in an unbalanced grid

The Dual Vector Current Control (DVCC) block detailed in the Figure 2-12 contains the current regulators for the dq currents of the positive and negative sequence. The outputs of the current controllers pass through the inverse Park transformation and are summed to give the final arm voltage references $\overrightarrow{u_{SM_{Li}}^{*}}$. This decoupling between the positive and negative sequences allows to control individually the two sequences.

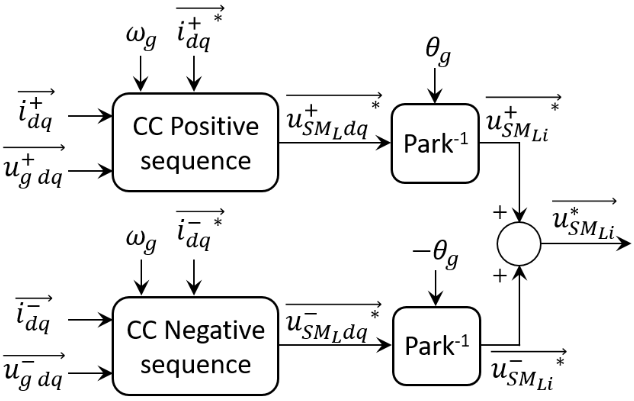

Figure 2-12 : Dual Vector Current Control (DVCC)

Finally, the energy control which generates the d-axes positive sequence reference i_d^{+*} and the calculation of the q-axes positive sequence reference i_q^{+*} are the same as for the balanced grid explain in the Figure 2-10. The dq-axes negative sequence references i_d^{-*} and i_q^{-*} depends of the application and will be discussed in more detail further in this report.

Note that the zero sequence of the currents and voltages are not used because the SSBC is not able to influence the zero sequence from the grid point of view. Indeed, the neutral point of the SSBC is not connected to the neutral point of the grid.

If the control scheme of the Figure 2-11 is used for unbalanced operation, it will not work properly due to unbalanced phase power exchange. As a matter of fact, the difficulty in an unbalanced grid for a STATCOM application with a MMCC topology comes from the lack of a common DC link in the system. This lack makes that it has no automatic energy exchange between the phase legs. Therefore, the unbalance grid leads to unbalanced phase power exchange and leads to cluster voltages $u_{SM_L}^{\Sigma}$ that will diverge. This complicates the control and need more sophisticated controller to exchange energy between the phase legs and (re)balance the cluster voltages $u_{SM_L}^{\Sigma}$.

As presented in [6], it is possible to balance the cluster voltage with 2 different control strategies. The first one is the Zero Sequence Voltage Control (ZSVC) and the second one is the Negative Sequence Current Control (NSCC). These two strategies are detailed in the two next sections and are called the clusters control.

2.6.1 Zero Sequence Voltage Control (ZSVC)

The objective of the ZSVC is to generate a zero sequence voltage to compensate the unbalanced phase power exchange coming from the unbalanced grid conditions. The basis of the development below comes from [4] and [6].

Let assume that all the quantities are sinusoidal. The SSBC exchange positive and negative sequence currents with the grid. The grid contains positive and negative sequence voltages. Thus, the SSBC will generate positive, negative and zero sequence arm voltages $\overrightarrow{u_{SM_{Li}}}$. These definitions are shown in the equations (2.24).

$$
\begin{gathered}
\underline{I}_{L_1} = \hat{I}_p \cdot e^{j\cdot\delta_p} + \hat{I}_n \cdot e^{j\cdot\delta_n} \\
\underline{I}_{L_2} = \hat{I}_p \cdot e^{j\cdot\left(\delta_p - \frac{2\cdot\pi}{3}\right)} + \hat{I}_n \cdot e^{j\cdot\left(\delta_n + \frac{2\cdot\pi}{3}\right)} \\
\underline{I}_{L_3} = \hat{I}_p \cdot e^{j\cdot\left(\delta_p + \frac{2\cdot\pi}{3}\right)} + \hat{I}_n \cdot e^{j\cdot\left(\delta_n - \frac{2\cdot\pi}{3}\right)} \\
\underline{U}_{SML1} = \widehat{U}_p \cdot e^{j\cdot\theta_p} + \widehat{U}_n \cdot e^{j\cdot\theta_n} + \widehat{U}_0 \cdot e^{j\cdot\alpha_0} \\
\underline{U}_{SML2} = \widehat{U}_p \cdot e^{j\cdot\left(\theta_p - \frac{2\cdot\pi}{3}\right)} + \widehat{U}_n \cdot e^{j\cdot\left(\theta_n + \frac{2\cdot\pi}{3}\right)} + \widehat{U}_0 \cdot e^{j\cdot\alpha_0} \\
\underline{U}_{SML3} = \widehat{U}_p \cdot e^{j\cdot\left(\theta_p + \frac{2\cdot\pi}{3}\right)} + \widehat{U}_n \cdot e^{j\cdot\left(\theta_n - \frac{2\cdot\pi}{3}\right)} + \widehat{U}_0 \cdot e^{j\cdot\alpha_0}
\end{gathered} \tag{2.24}
$$

The active power in each phase can be calculated by:

$$P_{L_i} = \Re\{\underline{S}_{L_i}\} = \Re\{\underline{U}_{SML_i} \cdot \underline{I}^*_{L_i}\} \tag{2.25}$$

Once the development is done and simplified, it is possible to define the zero sequence voltage to generate (amplitude and phase angle) which will lead to the desired unbalanced phase power exchange that will compensate the effects of the unbalanced conditions of the grid. This result is shown in the relation (2.26). For more details on the development, see appendix 9.1.

$$\begin{gathered} tan(\alpha_0) = \frac{(P_{imb\,L2} - K_2) \cdot K_3 - (P_{imb\,L1} - K_1) \cdot K_5}{(P_{imb\,L1} - K_1) \cdot K_6 - (P_{imb\,L2} - K_2) \cdot K_4} \\ \widehat{U}_0 = \frac{P_{imb\,L1} - K_1}{K_3 \cdot cos(\alpha_0) + K_4 \cdot sin(\alpha_0)} = \frac{P_{imb\,L2} - K_2}{K_5 \cdot cos(\alpha_0) + K_6 \cdot sin(\alpha_0)} \end{gathered} \tag{2.26}$$

with

$$\begin{gathered} K_1 = \frac{\widehat{U}_p \cdot \hat{I}_n}{2} \cdot cos(\theta_p - \delta_n) + \frac{\widehat{U}_n \cdot \hat{I}_p}{2} \cdot cos(\theta_n - \delta_p) \\ K_2 = \frac{\widehat{U}_p \cdot \hat{I}_n}{2} \cdot cos\left(\theta_p - \delta_n - \frac{4 \cdot \pi}{3}\right) + \frac{\widehat{U}_n \cdot \hat{I}_p}{2} \cdot cos\left(\theta_n - \delta_p + \frac{4 \cdot \pi}{3}\right) \\ K_3 = \frac{\hat{I}_n}{2} \cdot cos(\delta_n) + \frac{\hat{I}_p}{2} \cdot cos(\delta_p) \\ K_4 = \frac{\hat{I}_n}{2} \cdot sin(\delta_n) + \frac{\hat{I}_p}{2} \cdot sin(\delta_p) \\ K_5 = \frac{\hat{I}_n}{2} \cdot cos\left(\delta_n + \frac{2 \cdot \pi}{3}\right) + \frac{\hat{I}_p}{2} \cdot cos\left(\delta_p - \frac{2 \cdot \pi}{3}\right) \\ K_6 = \frac{\hat{I}_n}{2} \cdot sin\left(\delta_n + \frac{2 \cdot \pi}{3}\right) + \frac{\hat{I}_p}{2} \cdot sin\left(\delta_p - \frac{2 \cdot \pi}{3}\right) \end{gathered} \tag{2.27}$$

It is important to note that $P_{imb\,Li}$ will be defined by the clusters control and are derived from the difference between the arm energies.

Now, the control scheme of the SSBC in an unbalanced grid can be completed with the clusters control as shown in the Figure 2-13. The clusters control contains the ZSVC strategy and generates the zero sequence voltage which is added to the arm voltage references $\overrightarrow{u^*_{SM_{Li}}}$.

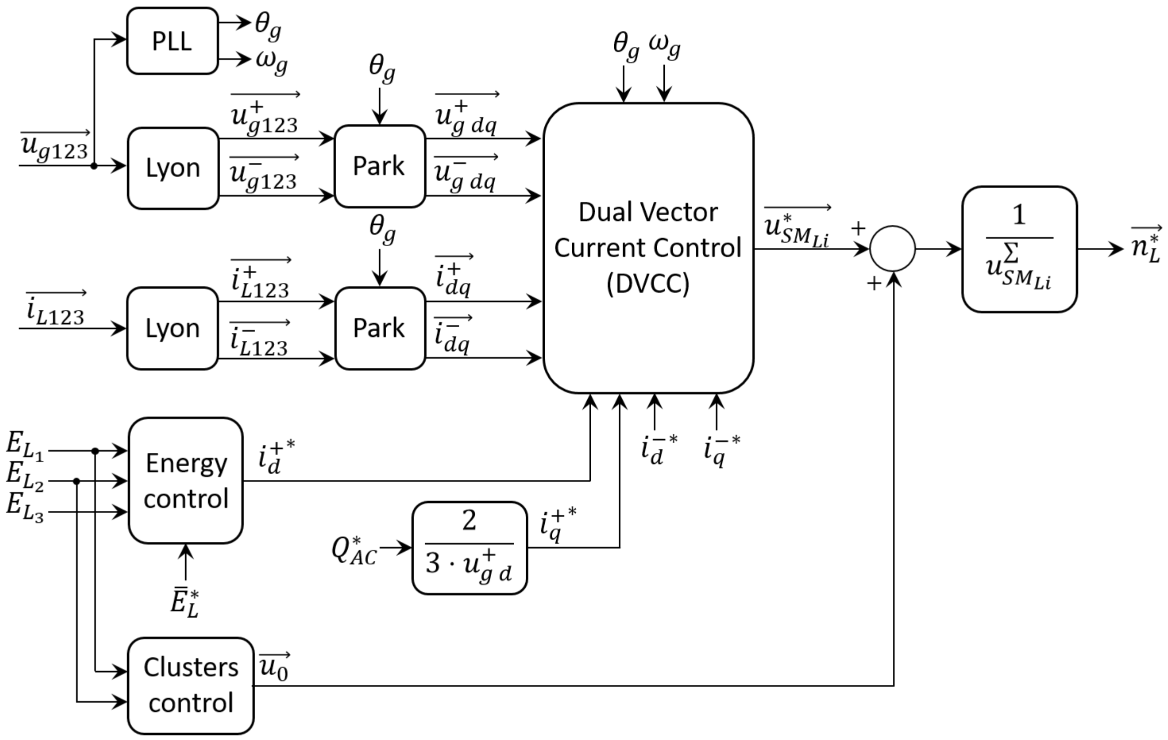

Figure 2-13 : Control scheme of the SSBC with ZSVC

The detail of the clusters control is shown on the Figure 2-14. The cluster regulators compare the arm energy average of one phase $\bar{E}_{L_i}$ with the global energy average of the three phases $\bar{E}_L$. The output of the regulators are the power imbalance $P^*_{imb\ L_i}$ to generate. Finally, the equations (2.26) and (2.27) are used to compute the amplitude and the phase angle of the zero sequence voltage to generate.

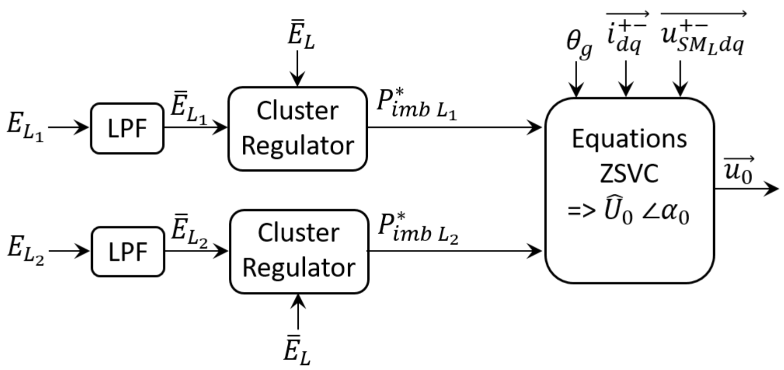

Figure 2-14 : Detail of the clusters control with the ZSVC strategy

2.6.1.1 Operating range of the ZSVC

The equations (2.26) which permit to compute the amplitude and the phase angle of the zero sequence voltage to generate are too complicated to understand on the first view how the results will change according to the conditions. The most limiting factor in the zero sequence voltage generation is its amplitude. From theses equations, it is noticeable that the amplitude may become infinite if the denominator is equal to zero. So it depends on the factors K_3 to K_6 and therefore on the positive and negative current amplitude. Thus, it is possible to say that the SSBC is mainly sensitive to the amount of positive and negative sequence currents that the converter exchange with the grid.

To visualise in a simple way, the approach is to compute the amplitude of the zero sequence voltage $\widehat{U}_0$ according to the amplitude of the positive and negative sequence currents under certain conditions of phase difference between the sequence currents. In [6], it is explain that the worst case (largest amplitude of the zero sequence voltage) is when $\delta_p = \delta_n = \pi/2$ and the best case is when $\delta_p = -\delta_n =$

$\pi/2$. Finally, the unbalanced power references $P^*_{imb\ L_i}$ must be fixed at a realistic value. In the Figure 2-15, $P^*_{imb\ L_1}$ is fixed to 0.02 [pu] and $P^*_{imb\ L_2}$ is set to 0.01 [pu]. These small values are choose to model the small disturbances caused by non-idealities.

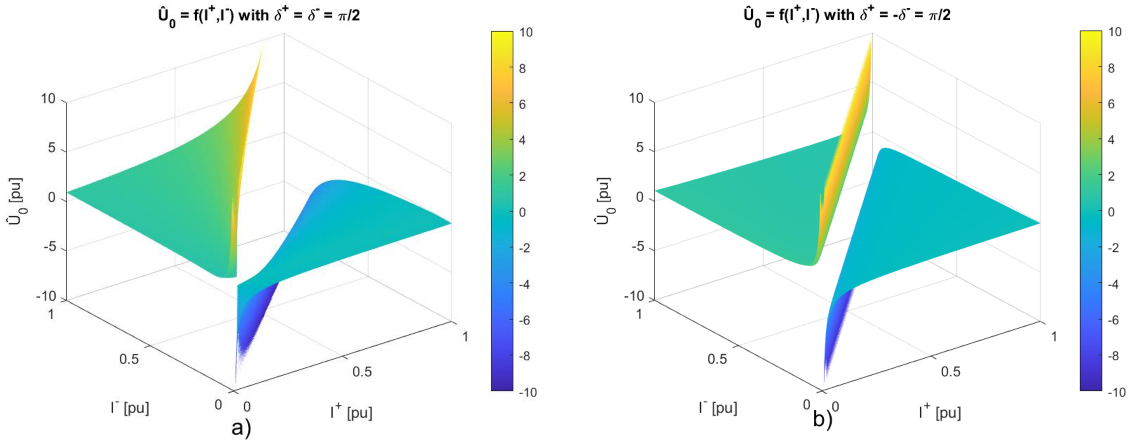

Figure 2-15 : Amplitude of the zero sequence voltage in the worst (a) and best (b) case

In the figure above, it is visible that the amplitude of the zero sequence voltage tends to infinity when the positive and negative sequence currents approach the same values. In addition, the amplitude is shown until a value of 10 [pu] which is much larger than the converter can deliver. Now, to better understand the operating range of the ZSVC, the same figures are flattened and shown in the Figure 2-16 with a maximum amplitude of 1 [pu].

The coloured parts are the amplitudes which are between ±1 [pu]. The white parts are when the amplitudes are larger than ±1 [pu] and therefore the converter is not able to operate at these operating points.

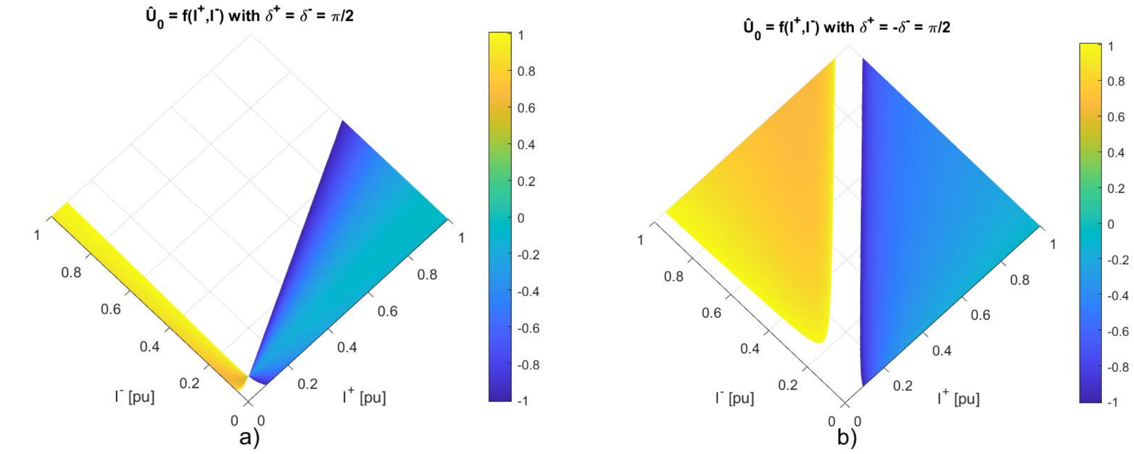

Figure 2-16 : Amplitude of the zero sequence voltage in the worst (a) and best (b) case (flattened view)

In the best case, the converter is able to work at a majority of operating points. On the other hand, in the worst case, it has a majority of operating points where the converter will not be able to generate the correct amplitude of the zero sequence voltage. Note that if the currents are null, it is impossible to generate imbalanced power and therefore impossible to (re)balance the cluster voltages.

As a conclusion for the operating range of the SSBC with the ZSVC strategy, it is important to note that according the amplitude and difference of phase of the positive and negative sequence currents, the converter will not always be able to work correctly and so not able to (re)balanced the cluster voltages $u^{\Sigma}_{SM_L}$.

2.6.2 Negative Sequence Current Control (NSCC)

The objective of the NSCC is to control the negative sequence current that the STATCOM exchanges with the grid to rebalance the cluster voltages. Note that if the negative sequence current is used for the rebalanced control, it is logically impossible to do load balancing.

From [6], the amplitude and phase angle of the negative sequence current to generate are presented in the equation (2.28).

$$tan(\delta_n) = \frac{(P_{imb\,L2} - K_{i2}) \cdot K_{i3} - (P_{imb\,L1} - K_{i1}) \cdot K_{i5}}{(P_{imb\,L1} - K_{i1}) \cdot K_{i6} - (P_{imb\,L2} - K_{i2}) \cdot K_{i4}}$$

$$\hat{I}_n = \frac{P_{imb\,L1} - K_{i1}}{K_{i3} \cdot cos(\delta_n) + K_{i4} \cdot sin(\delta_n)} = \frac{P_{imb\,L2} - K_{i2}}{K_{i5} \cdot cos(\delta_n) + K_{i6} \cdot sin(\delta_n)} \tag{2.28}$$

with

$$K_{i1} = \frac{\hat{U}_n \cdot \hat{I}_p}{2} \cdot cos(\theta_n - \delta_p), \qquad K_{i2} = \frac{\hat{U}_n \cdot \hat{I}_p}{2} \cdot cos\left(\theta_n - \delta_p + \frac{4 \cdot \pi}{3}\right)$$

$$K_{i3} = \frac{\hat{U}_p}{2} \cdot cos(\theta_p), \qquad K_{i4} = \frac{\hat{U}_p}{2} \cdot sin(\theta_p) \tag{2.29}$$

$$K_{i5} = \frac{\hat{U}_p}{2} \cdot cos\left(\theta_p - \frac{4 \cdot \pi}{3}\right), \qquad K_{i6} = \frac{\hat{U}_p}{2} \cdot sin\left(\theta_p - \frac{4 \cdot \pi}{3}\right)$$

The result is of the same form that for the ZSVC strategy. Now, neglecting $P_{imb\,Li}$ for simpler analysis, the negative sequence current amplitude and phase angle are in a simpler form as shown in equation (2.30).

$$\delta_n = -\delta_p + \theta_n + \theta_p + \pi$$

$$\hat{I}_n = \frac{\hat{U}_n \cdot \hat{I}_p}{\hat{U}_p} \tag{2.30}$$

So, the condition $\hat{U}_n = \hat{U}_p$ yields to $\hat{I}_n = \hat{I}_p$ and this could cause problems in the control. Actually, to compensate the system losses, the energy controller will generate a three-phase active power of $\frac{3}{2} \cdot \hat{U}_p \cdot \hat{I}_p \cdot \cos(\theta_p - \delta_p)$. Unfortunately, the NSCC will generate three-phase active power of $\frac{3}{2} \cdot \hat{U}_n \cdot \hat{I}_n \cdot \cos(\theta_n - \delta_n)$. Therefore, under this condition, it is possible that the NSCC power generation will cancel the power generation demand from the energy controller. So, NSCC must be avoided if the condition $\hat{U}_n = \hat{U}_p$ is possible to appear.

3 SINGLE DELTA BRIDGE-CELLS (SDBC)

The schematic of the SDBC structures is visible on the Figure 3-1. This topology is interesting because it has an internal circulating current which helps the control at zero power exchange. On the other hand, this structure need $\sqrt{3}$ more cells to support the higher voltage.

This system is suitable to exchange a controlled reactive power and to mitigate the flicker effect. The cells in the figure below are the same as for the SSBC structure presented in the chapter 2.

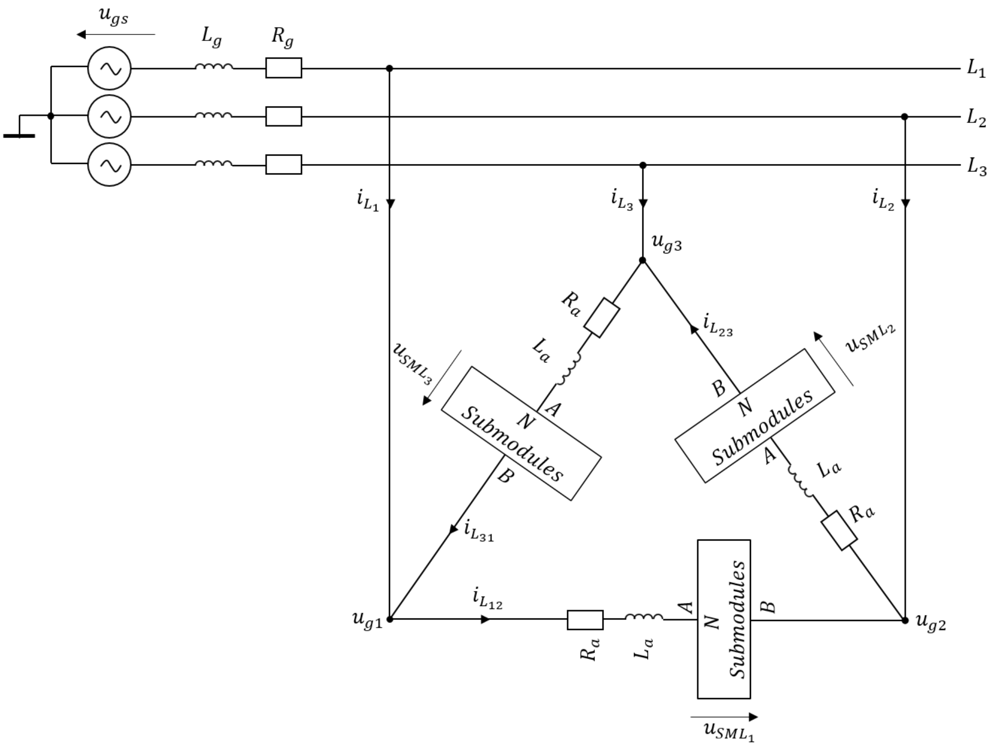

Figure 3-1 : SDBC schematic

To simplify the analysis, as done for the SSBC, the single-phase schematic as seen on the Figure 3-2 is used. The analysis being quite the same as this of the SSBC presented in the chapter 2, the development is simplified. It is important to note that the voltage that the cells must support are $\sqrt{3}$ higher in this case.

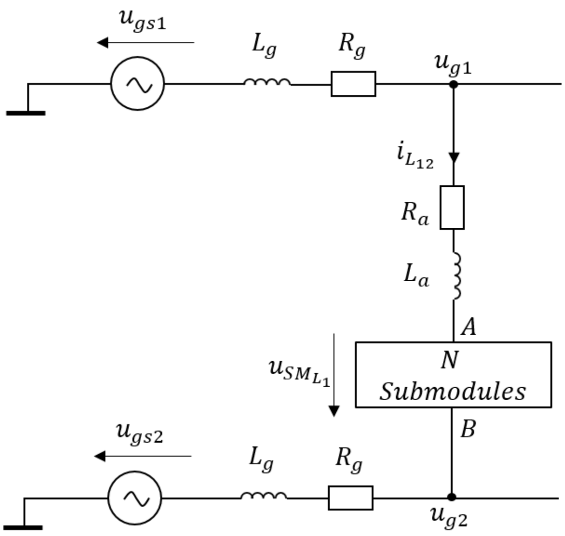

Figure 3-2 : Single phase schematic of the SDBC

3.1 System model

Following the same steps as for the SSBC in chapters 2.1 and 2.2, the block diagram of the whole system model is shown in Figure 3-3. The only difference with the SSBC structure is value of the grid voltage (line voltage instead of the phase voltage).

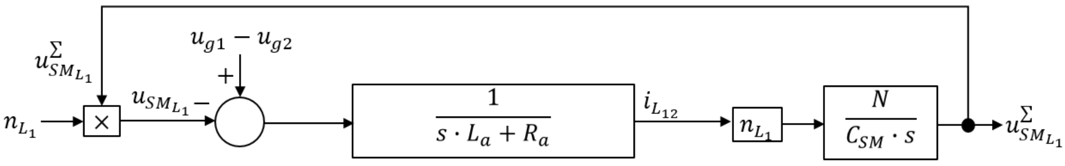

Figure 3-3 : Block diagram of the SDBC system model

3.2 Control of the system

The complete control scheme of the SDBC is quite the same as for the SSBC and is shown in Figure 3-4. The differences are not visible on this scheme, they are:

- If the capacity of each cell is the same as in the SSBC, the energy reference $\bar{E}_L^*$ must be 3 times higher because the cluster voltages $u^{\Sigma}_{SM_{Li}}$ are $\sqrt{3}$ times higher.
- The Park inverse transformation (dq -> abc) must use a transformation angle of θ + π/6 and an amplification factor of $\sqrt{3}$.

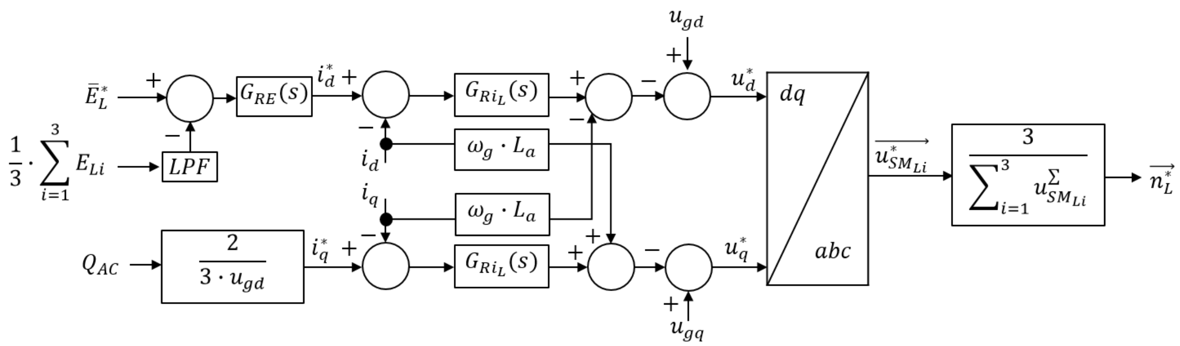

Figure 3-4 : Complete control scheme of the SDBC in a balanced grid

3.3 Unbalanced grid

As the SSBC, the SDBC has to continue to operate properly even if the grid is unbalanced or if a fault occurs in the grid. The same methods are used to do the control. For more details, refer to the section 2.6.

3.3.1 Zero Sequence Current Control (ZSCC)

The objective of the ZSCC is to generate a zero sequence current to compensate the unbalanced phase power exchange coming from the unbalanced grid conditions. The basis of the development below comes from [4] and [6].

Let assume that all the quantities are sinusoidal. The SDBC exchange positive and negative sequence currents with the grid. The grid contains positive and negative sequence voltages. Moreover the converter generates an internal zero sequence current. These definitions are shown in the equations (3.1).

$$
\begin{aligned}
\underline{I}_{L_{12}} &= \hat{I}_p \cdot e^{j \cdot \delta_p} + \hat{I}_n \cdot e^{j \cdot \delta_n} + \hat{I}_0 \cdot e^{j \cdot \delta_0} \\
\underline{I}_{L_{23}} &= \hat{I}_p \cdot e^{j \cdot \left(\delta_p - \frac{2 \cdot \pi}{3}\right)} + \hat{I}_n \cdot e^{j \cdot \left(\delta_n + \frac{2 \cdot \pi}{3}\right)} + \hat{I}_0 \cdot e^{j \cdot \delta_0}
\end{aligned}
\tag{3.1}
$$

$$\underline{I}_{L_{31}} = \hat{I}_p \cdot e^{j\cdot\left(\delta_p+\frac{2\cdot\pi}{3}\right)} + \hat{I}_n \cdot e^{j\cdot\left(\delta_n-\frac{2\cdot\pi}{3}\right)} + \hat{I}_0 \cdot e^{j\cdot\delta_0}$$

$$\underline{U}_{SML1} = \widehat{U}_p \cdot e^{j\cdot\theta_p} + \widehat{U}_n \cdot e^{j\cdot\theta_n}$$

$$\underline{U}_{SML2} = \widehat{U}_p \cdot e^{j\cdot\left(\theta_p-\frac{2\cdot\pi}{3}\right)} + \widehat{U}_n \cdot e^{j\cdot\left(\theta_n+\frac{2\cdot\pi}{3}\right)}$$

$$\underline{U}_{SML3} = \widehat{U}_p \cdot e^{j\cdot\left(\theta_p+\frac{2\cdot\pi}{3}\right)} + \widehat{U}_n \cdot e^{j\cdot\left(\theta_n-\frac{2\cdot\pi}{3}\right)}$$

The active power in each arm can be calculated by:

$$P_{L_{ij}} = \Re\left\{\underline{S}_{L_{ij}}\right\} = \Re\left\{\underline{U}_{SML_i} \cdot \underline{I}^*_{L_{ij}}\right\} \tag{3.2}$$

Once the development is done and simplified, it is possible to define the zero sequence curent to generate (amplitude and phase angle) which will lead to the desired unbalanced phase power exchange that will compensate the effects of the unbalanced conditions of the grid. This result is shown in the relation (3.3). For more details on the development, see appendix 9.2.

$$\begin{gathered} tan(\delta_0) = \frac{(P_{imb\,L23} - K_{12}) \cdot K_{13} - (P_{imb\,L12} - K_{11}) \cdot K_{15}}{(P_{imb\,L12} - K_{11}) \cdot K_{16} - (P_{imb\,L23} - K_{12}) \cdot K_{14}} \\ \hat{I}_0 = \frac{P_{imb\,L12} - K_{11}}{K_{13} \cdot cos(\delta_0) + K_{14} \cdot sin(\delta_0)} = \frac{P_{imb\,L23} - K_{12}}{K_{15} \cdot cos(\delta_0) + K_{16} \cdot sin(\delta_0)} \end{gathered} \tag{3.3}$$

with

$$\begin{gathered} K_{11} = \frac{\widehat{U}_p \cdot \hat{I}_n}{2} \cdot cos(\theta_p - \delta_n) + \frac{\widehat{U}_n \cdot \hat{I}_p}{2} \cdot cos(\theta_n - \delta_p) \\ K_{12} = \frac{\widehat{U}_p \cdot \hat{I}_n}{2} \cdot cos\left(\theta_p - \delta_n - \frac{4\cdot\pi}{3}\right) + \frac{\widehat{U}_n \cdot \hat{I}_p}{2} \cdot cos\left(\theta_n - \delta_p + \frac{4\cdot\pi}{3}\right) \\ K_{13} = \frac{\widehat{U}_n}{2} \cdot cos(\theta_n) + \frac{\widehat{U}_p}{2} \cdot cos(\theta_p) \\ K_{14} = \frac{\widehat{U}_n}{2} \cdot sin(\theta_n) + \frac{\widehat{U}_p}{2} \cdot sin(\theta_p) \\ K_{15} = \frac{\widehat{U}_n}{2} \cdot cos\left(\theta_n + \frac{2\cdot\pi}{3}\right) + \frac{\widehat{U}_p}{2} \cdot cos\left(\theta_p - \frac{2\cdot\pi}{3}\right) \\ K_{16} = \frac{\widehat{U}_n}{2} \cdot sin\left(\theta_n + \frac{2\cdot\pi}{3}\right) + \frac{\widehat{U}_p}{2} \cdot sin\left(\theta_p - \frac{2\cdot\pi}{3}\right) \end{gathered} \tag{3.4}$$

It is important to note that $P_{imb\,Lij}$ will be defined by the clusters control and are derived from the difference between the arm energies.

Now, the control scheme of the SDBC in an unbalanced grid can be completed with the clusters control as shown in the Figure 3-5. The clusters control contains the ZSCC strategy and generates the zero sequence current. It has two principal differences with the SSBC control scheme of the Figure 2-13:

1. The angle θ_g and the amplitude in the output generation of the DVCC must take in count the fact that it works in a delta configuration. So the angle must be $\theta_g + \pi/6$ and the amplitudes must be multiplied by $\sqrt{3}$.
2. Unlike to ZSVC, the zero sequence cannot directly be added to the output from the DVCC. Here, the zero sequence voltage that leads to the desired zero sequence current is generated through a proportional controller with a K_{i_0} gain.

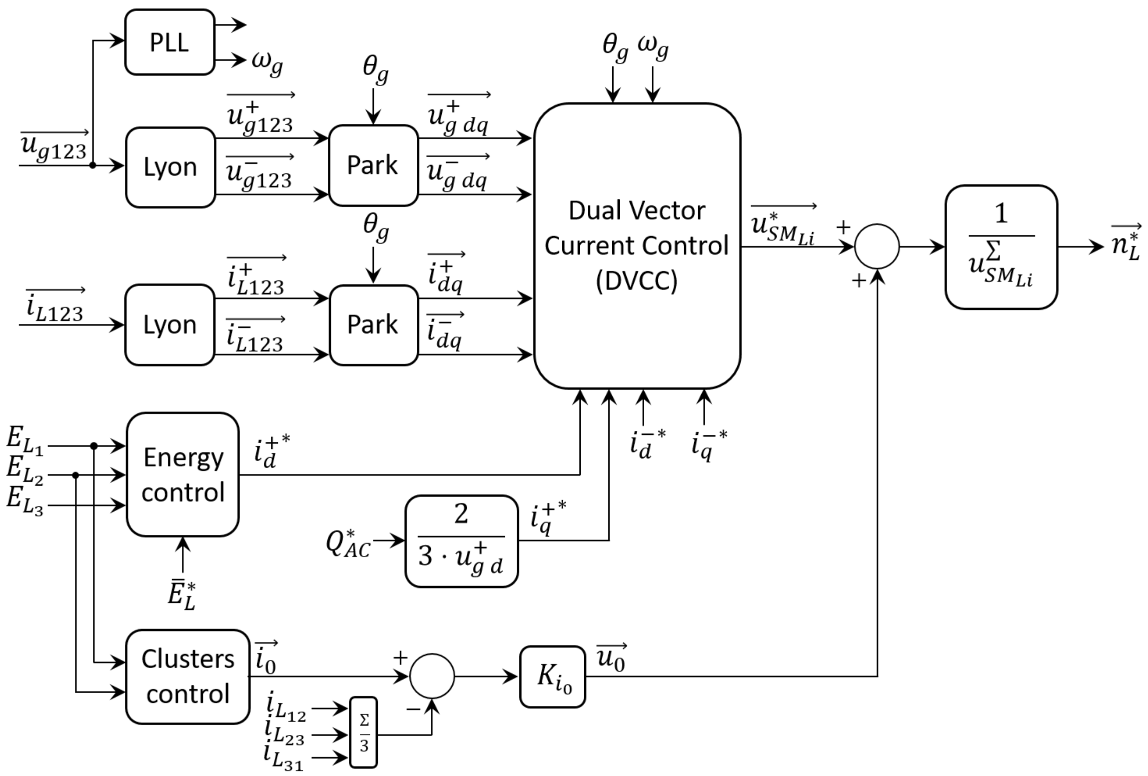

Figure 3-5 : Control scheme of the SDBC with ZSCC

The detail of the clusters control is shown on the Figure 3-6. Its operation is the same as for the SSBC. Just the equations to generate the zero sequence current $\vec{i_0}$ is different and refer to equations (3.3) and (3.4).

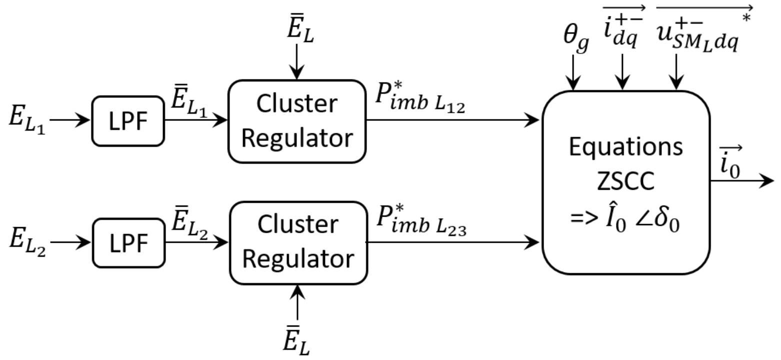

Figure 3-6 : Detail of the clusters control with the ZSCC

3.3.1.1 *Operating range of the ZSCC*

The equations (3.3) which permits to compute the amplitude and the phase angle of the zero sequence current to generate are too complicated to understand on the first view how the results will change according to the conditions. The most limiting factor in the zero sequence current generation is its amplitude. From these equations, it is noticeable that the amplitude may become infinite if the denominator is equal to zero. So it depends on the factors K_{13} to K_{16} and therefore on the positive and negative sequence voltages amplitude.

To visualise in a simple way, the approach is to compute the amplitude of the zero sequence current $\hat{I}_0$ according to the amplitude of the positive and negative sequence voltages under certain conditions of phase difference between the sequence voltages. In [6], it is explain that the worst case (largest amplitude of the zero sequence current) is when $\theta_p = \theta_n = 0$ and the best case is when $\theta_p = 0,\ \theta_n = \pi$. Finally, as for the ZSVC strategy, the unbalanced power references $P^*_{imb\ L_{ij}}$ must be fixed at a realistic value. In the Figure 3-7, $P^*_{imb\ L_{12}}$ is fixed to 0.02 [pu] and $P^*_{imb\ L_{23}}$ is set to 0.01 [pu]. These small values are choose to model the small disturbances caused by non-idealities.

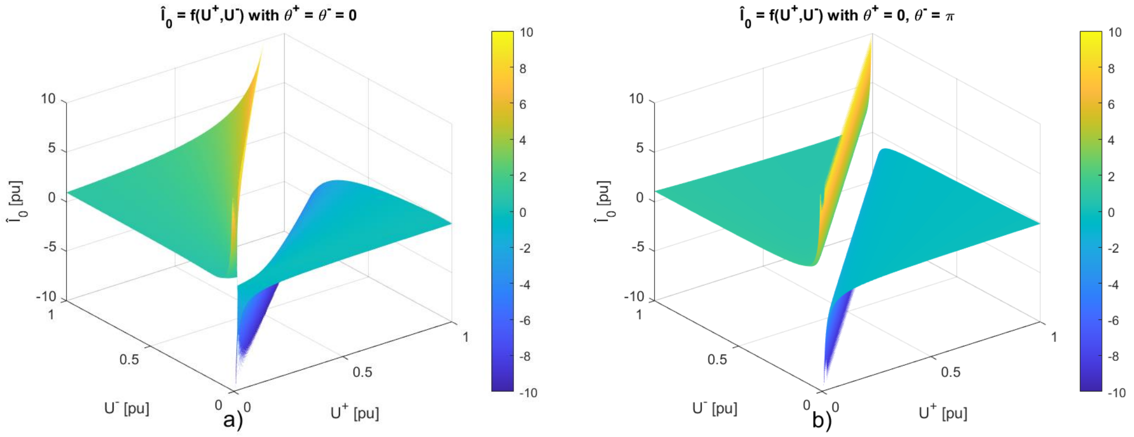

Figure 3-7 : Amplitude of the zero sequence current in the worst (a) and best (b) case

In the figure above, it is visible that the amplitude of the zero sequence current tends to infinity when the positive and negative sequence voltages approach the same values. In addition, the amplitude is shown until a value of 10 [pu] which is much larger than the converter can deliver. Now, to better understand the operating range of the ZSVC, the same figures are flattened and shown in the Figure 3-8 with a maximum amplitude of 1 [pu].

The coloured parts are the amplitudes which are between ±1 [pu]. The white parts are when the amplitudes are larger than ±1 [pu] and therefore the converter is not able to operate at these operating points.

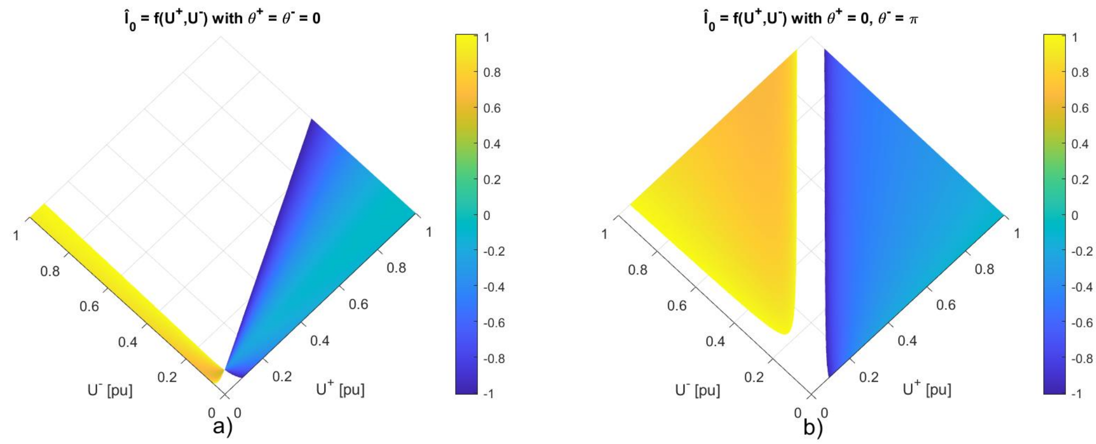

Figure 3-8 : Amplitude of the zero sequence current in the worst (a) and best (b) case (flattened view)

In the best case, the converter is able to work at a majority of operating points. On the other hand, in the worst case, it has a majority of operating points where the converter will not be able to generate the correct amplitude of the zero sequence current. Note that if the voltages are null, it is impossible to generate imbalanced power and therefore impossible to (re)balance the cluster voltages.

As a conclusion for the operating range of the SDBC with the ZSCC strategy, it is important to note that according the amplitude and difference of phase of the positive and negative sequence voltages, the converter will not always be able to work correctly and so not able to (re)balanced the cluster voltages $u^{\Sigma}_{SM_L}$.

It is also interesting to see that the operating range of the ZSCC is exactly the same as the ZSVC if we replace the current sequences by the voltage sequences.

3.3.2 Negative Sequence Current Control

The negative sequence current control works exactly the same as for the SSBC. In [6], the amplitude and phase angle of the negative sequence current to generate are presented. In this case, the computation is exactly the same as for the SSBC structure. So, refer to the equations (2.28) and (2.29).

The conclusion presented at the end of the section 2.6.2 is therefore the same here. If $\hat{U}_n = \hat{U}_p$, it is possible that the NSCC power generation will cancel the power generation demand from the energy controller. So, NSCC must be avoided if this condition can appear.

4 DOUBLE STAR CHOPPER-CELLS (DSCC)

Despite its higher number of submodules and thus its lower power density, the circulating current and high modularity make this topology interesting to compare with the SDBC and SSBC presented above in this report, especially concerning grid unbalanced management and zero power exchange. The schematic of the DSCC structures is visible on the Figure 4-1.

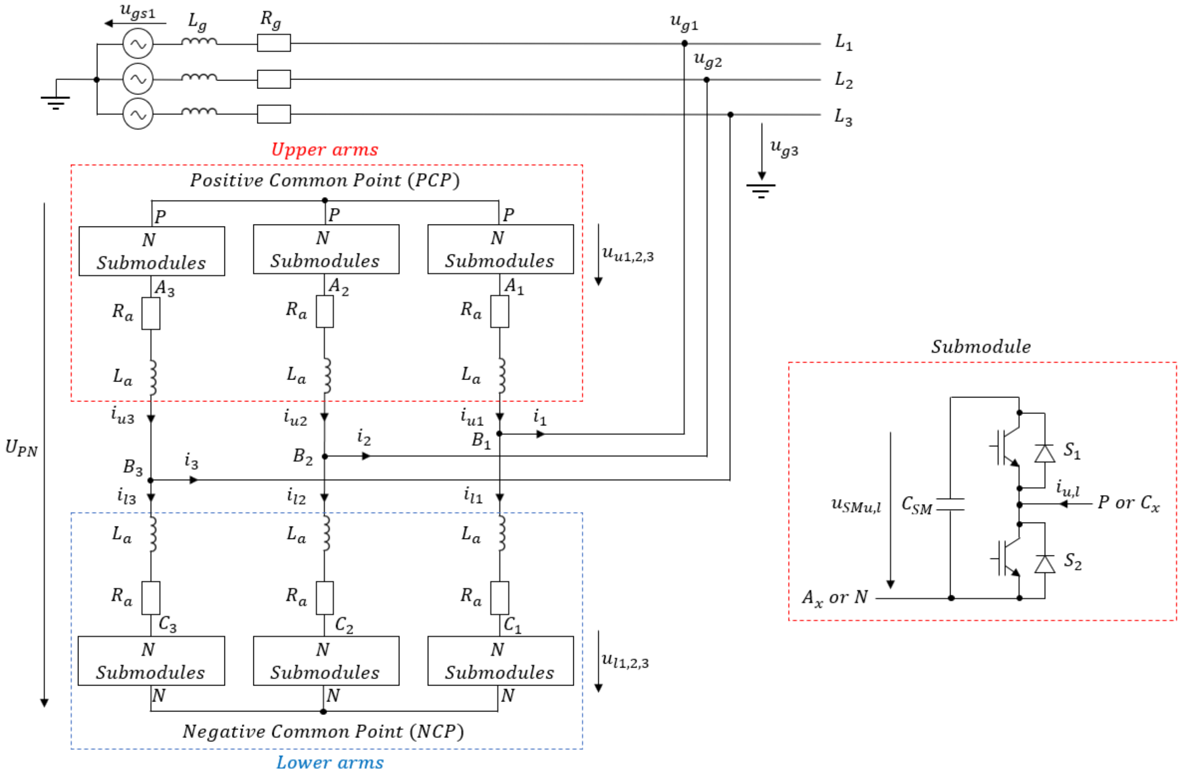

Figure 4-1 : DSCC (Double-Star Chopper-Cell) STATCOM schematic with Half-Bridge submodules

4.1 CONVERTER MODELLING

DSCC topology is analysed to obtain its equivalent block diagram model. This block diagram is used to design the control for a STATCOM application in 3-phase balanced grid operation. Given that the system is considered balanced, a per phase analysis can be performed. Figure 4-2 shows the new schematic used in the next sections. Indexes 1, 2 and 3 are not mentioned anymore to simplify the reading.

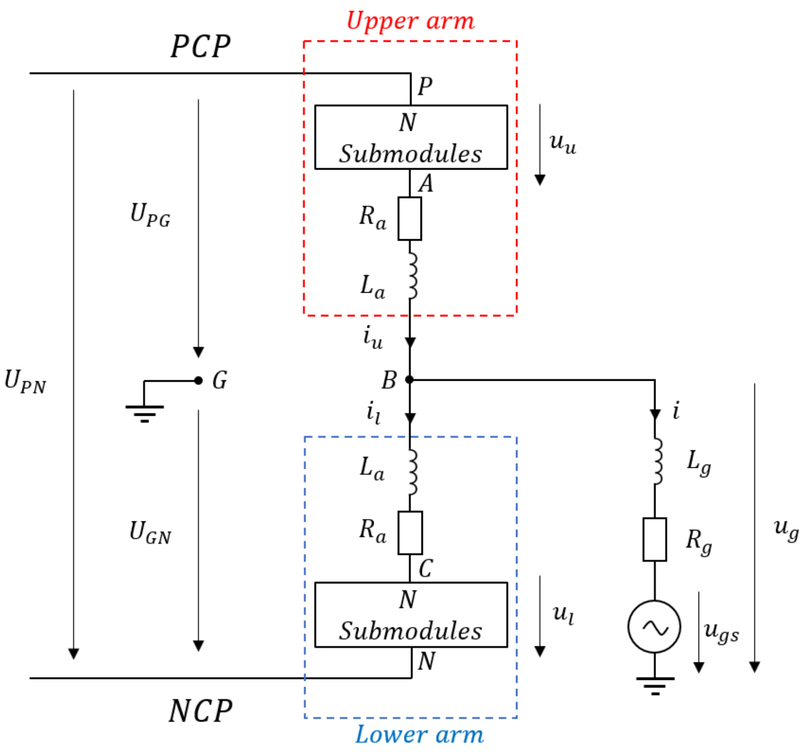

Figure 4-2: DSCC (Double-Star Chopper-Cell) STATCOM per phase analysis schematic

4.1.1 Output voltage and current relationship

Kirchhoff's Current Law (KCL) applied to point B gives relation (3.1).

$$i = i_u - i_l \tag{3.1}$$

Applying Kirchhoff's Voltage Law (KVL) to upper arm, (3.2) is obtained.

$$u_{gs} = -R_g \cdot i - L_g \cdot \frac{\partial i}{\partial t} - R_a \cdot i_u - L_a \cdot \frac{\partial i_u}{\partial t} - u_u + U_{PG} \tag{3.2}$$

Applying Kirchhoff's Voltage Law (KVL) to lower arm, (3.3) is obtained.

$$u_{gs} = -R_g \cdot i - L_g \cdot \frac{\partial i}{\partial t} + R_a \cdot i_l + L_a \cdot \frac{\partial i_l}{\partial t} + u_l - U_{GN} \tag{3.3}$$

Adding (3.2) with (3.3) and considering (3.1) leads to (3.4).

$$\boxed{(3.2) + (3.3)\ \&\ (3.1)} \Rightarrow u_{gs} = -\left(R_g + \frac{R_a}{2}\right) \cdot i - \left(L_g + \frac{L_a}{2}\right) \cdot \frac{\partial i}{\partial t} + \frac{u_l - u_u}{2} + \frac{U_{PG} - U_{GN}}{2} \tag{3.4}$$

One objective of the control is to keep $\overline{U_{PN}}$ (average value of U_{PN}) to a constant value U_{DC} by the total energy controller. Small ripples still exist but are small compared with mean value. This is why they are neglected, leading to (3.5).

$$U_{PN} \approx \overline{U_{PN}} = U_{DC} \tag{3.5}$$

With balanced grid operation and considering (3.5), equation (3.6) can be written.

$$U_{PG} \approx U_{GN} \approx \frac{U_{DC}}{2} \tag{3.6}$$

In (3.4), u_g is given by (3.7).

$$u_g = \frac{u_l - u_u}{2} \tag{3.7}$$

Injecting (3.5), (3.6) and (3.7) in (3.4) simplifies to (3.8).

$$\boxed{(3.4)\&(3.5)\ \&(3.6)\&(3.7)} \Rightarrow u_{gs} = -\left(R_g + \frac{R_a}{2}\right) \cdot i - \left(L_g + \frac{L_a}{2}\right) \cdot \frac{\partial i}{\partial t} + u_g \tag{3.8}$$

Using Laplace transform on equation (3.8) leads to transfer function linking output current with output voltage. This transfer function is shown in Figure 4-3.

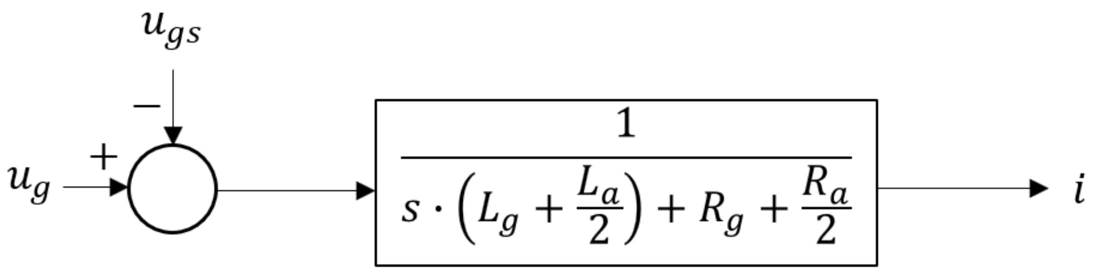

Figure 4-3: Outputs block diagram

4.1.2 Circulating voltage and current relationship

By subtracting (3.2) to (3.3) considering (3.6) and dividing everything by 2, relation (3.9) is obtained.

$$\boxed{(3.3) - (3.2)\ \&\ (3.6)} \Rightarrow 0 = R_a \cdot \frac{i_u + i_l}{2} + L_a \cdot \frac{\partial}{\partial t}\left(\frac{i_u + i_l}{2}\right) + \frac{u_u + u_l}{2} - \frac{U_{DC}}{2} \tag{3.9}$$

Circulating current et voltage are defined in (3.10) and (3.11) respectively.

$$i_{circ} = \frac{i_u + i_l}{2} \tag{3.10}$$

$$u_{circ} = \frac{u_u + u_l}{2} \tag{3.11}$$

Injecting (3.10) and (3.11) in (3.9) gives (3.12).

$$\boxed{(3.9)\&(3.10)\&(3.11)} \Rightarrow u_{circ} = \frac{U_{dc}}{2} - R_a \cdot i_{circ} - L_a \cdot \frac{\partial i_{circ}}{\partial t} \tag{3.12}$$

Using Laplace transform on equation (3.12) leads to block diagram linking circulating current with circulating voltage, shown in Figure 4-4.

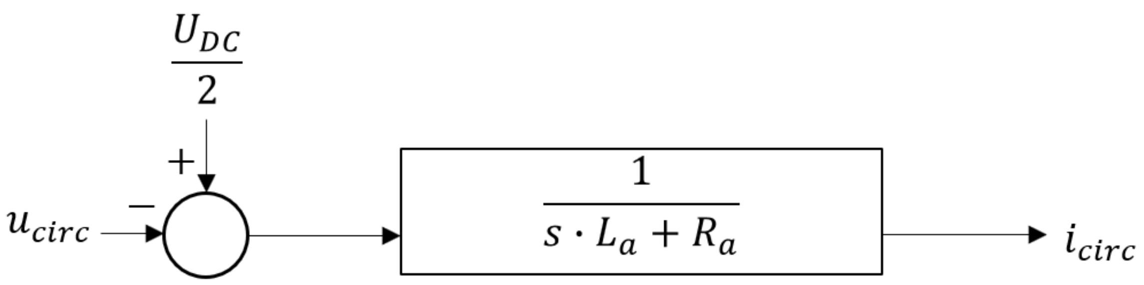

Figure 4-4: Circulating block diagram

4.1.3 Arms voltages and currents

It is possible to write arm currents as a function of output and circulating currents. (3.13) and (3.14) give arm current thanks to (3.1) and (3.10).

$$\boxed{(3.1)\ \&\ (3.10)} \Rightarrow i_u = i_{circ} + \frac{i}{2} \tag{3.13}$$

$$\boxed{(3.1)\ \&(3.10)} \Rightarrow i_l = i_{circ} - \frac{i}{2} \tag{3.14}$$

Thanks to (3.7) and (3.11), arm voltages are given as a function of output and circulating voltages in (3.15) and (3.16).

$$\boxed{(3.7)\ \&\ (3.11)} \Rightarrow u_u = u_{circ} - u_g \tag{3.15}$$

$$\boxed{(3.7)\ \&\ (3.11)} \Rightarrow u_l = u_{circ} + u_g \tag{3.16}$$

Finally, thanks to equations (3.7), (3.11), (3.13) and (3.14) as well as figures Figure 4-3 and Figure 4-4, relationship between arm voltages and arm currents can be modelled by the block diagram in Figure 4-5

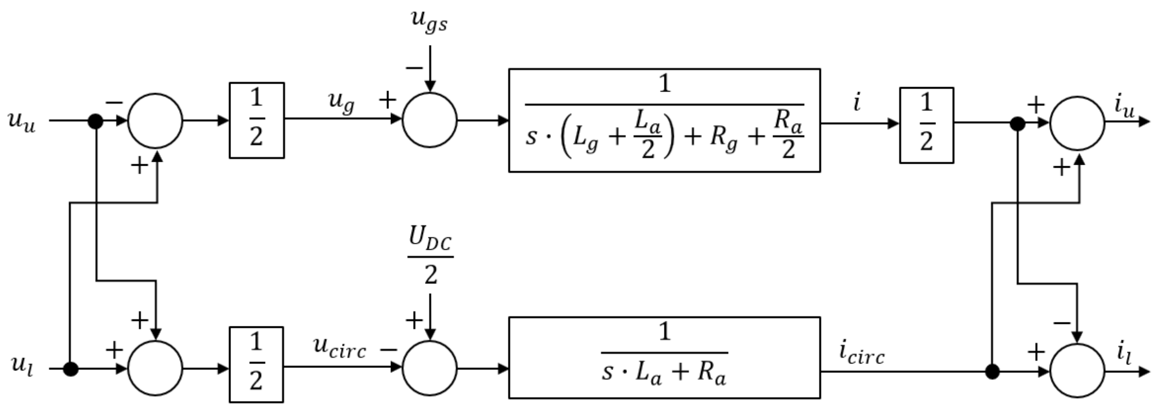

.

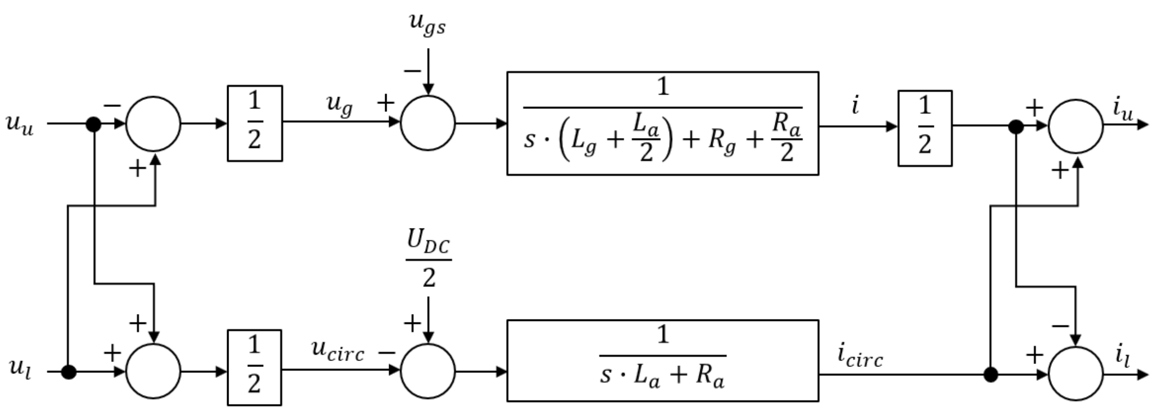

Figure 4-5: Relationship between arms currents and voltages

4.1.4 Insertion indices

As well as for SSBC and SDBC, it is necessary to include insertion indices to complete the modelling of the 3-wire DSCC converter. In this topology, submodules consist of half-bridge circuits employing 2 semiconductors with an anti-parallel-connected diode and a capacitor connected across both semiconductors as shown in Figure 4-6.

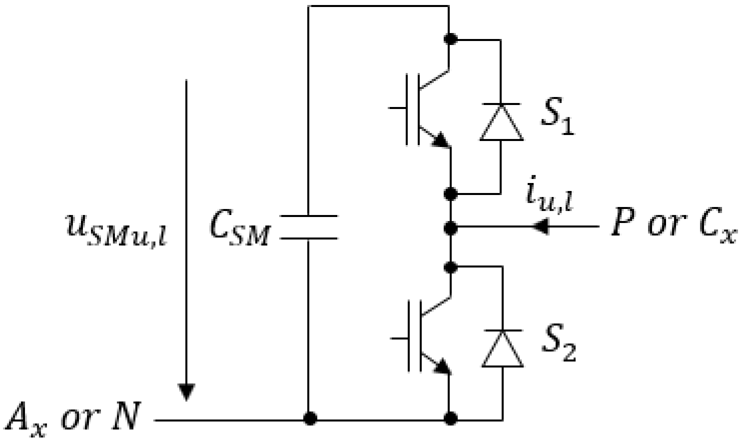

Figure 4-6: Half bridge submodule

Submodule insertion index $n_{u,l}^{i}$ can have only 2 values: 0 ou 1. If value is 0, the capacitor C_{SM} is bypassed, meaning that S_1 is « *OFF* » and S_2 is « *ON* » (Figure 4-6). If value is 1, the capacitor C_{SM} is inserted in the arm circuit, meaning that S_1 is « *ON* » and S_2 is « OFF » (Figure 4-6). In this case, capacitor is charging or discharging, depending on the direction of the arm current.

Thanks to this insertion index, it is possible to evaluate u_u and u_l by the values of $u_{SM_i u,l}$ which are the voltage of each submodule capacitor of one leg. To manage the DSCC control correctly, average voltage of each submodule capacitor C_{SM} has to be equal. It allows approximation proposed in (3.17).

$$u_{u,l} = \sum_{i=1}^{N} n_{u,l}^{i} \cdot u_{SM_i u,l} \cong \sum_{i=1}^{N} n_{u,l}^{i} \cdot \frac{u_{SMu,l}^{\Sigma}}{N} = \frac{u_{SMu,l}^{\Sigma}}{N} \cdot \sum_{i=1}^{N} n_{u,l}^{i} \tag{3.17}$$

In (3.17), $u_{SMu,l}^{\Sigma}$ represents the sum of submodules voltages of one arm when all submodules are inserted while N is the total number of submodules by arm.

(3.18) determines the number of submodules inserted by arm in [p.u.], called arm insertion index. There are N+1 possible values between 0 and 1 where 0 means all capacitors are bypassed and 1 means they are all inserted.

$$n_{u,l} = \frac{1}{N} \cdot \sum_{i=1}^{N} n_{u,l}^{i} \tag{3.18}$$

This arm insertion index in (3.18) allows to simplify expression (3.17) in (3.19).

$$\boxed{(3.17)\ \&(3.18)} \Rightarrow u_{u,l} = n_{u,l} \cdot u_{SMu,l}^{\Sigma} \tag{3.19}$$

Based on the fundamental equation linking current and voltage in a capacitor, (3.20) describes the current in a submodule. $n_{u,l}^{i}$ is present because if a capacitor is bypassed, its current is 0 [A].

$$n_{u,l}^{i} \cdot i_{u,l} = C_{SM} \cdot \frac{\partial u_{SM_i u,l}}{\partial t} \quad with\ index\ \ i = 1,2,\dots,N \tag{3.20}$$

As DSCC is composed of submodules in series, $i_{u,l}$ depends on the number of active submodules. It leads to (3.21).

$$C_{SM} \cdot \sum_{i=1}^{N} \frac{\partial u_{SM_i u,l}}{\partial t} = i_{u,l} \cdot \sum_{i=1}^{N} n_{u,l}^{i} \tag{3.21}$$

Using (3.18), it is possible to simplify (3.21) in (3.22).

$$\boxed{(3.18)\ \&\ (3.21)} \Rightarrow C_{SM} \cdot \sum_{i=1}^{N} \frac{\partial u_{SM_i u,l}}{\partial t} = i_{u,l} \cdot N \cdot n_{u,l} \tag{3.22}$$

(3.22) can be simplified in (3.23).

$$\frac{C_{SM}}{N} \cdot \frac{\partial u_{SMu,l}^{\Sigma}}{\partial t} = i_{u,l} \cdot n_{u,l} \tag{3.23}$$

By injecting (3.13) in (3.23), (3.24) is obtained.

$$\boxed{(3.13)\ \&\ (3.23)} \Rightarrow \frac{C_{SM}}{N} \cdot \frac{\partial u_{SMu}^{\Sigma}}{\partial t} = n_u \cdot \left(i_{circ} + \frac{i}{2}\right) \tag{3.24}$$

By injecting (3.14)(3.13) in (3.23), (3.25) is obtained.

$$\boxed{(3.14)\ \&\ (3.23)} \Rightarrow \frac{C_{SM}}{N} \cdot \frac{\partial u_{SMl}^{\Sigma}}{\partial t} = n_l \cdot \left(i_{circ} - \frac{i}{2}\right) \tag{3.25}$$

Utilizing (3.19), (3.24), (3.25) and the Figure 4-5, it is possible to establish the total DSCC block diagram shown in Figure 4-7. This block diagram is used to design the control of the DSCC.

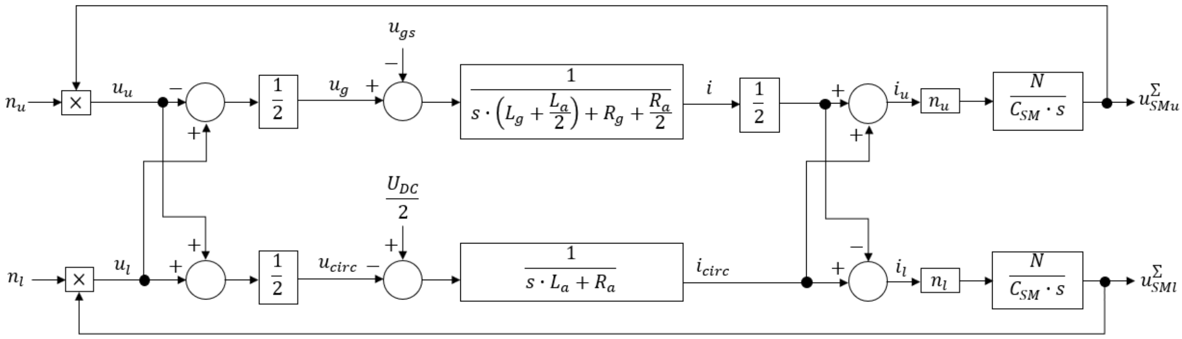

Figure 4-7: DSCC converter complete block diagram

4.2 Converter control in balanced grid

4.2.1 Overall control in balanced grid

The purpose of the converter control is to insure a control of reactive power injected in the PCC by following the reference Q^*. In the same time, the voltages of the capacitors have to be maintained and balanced in each arm, between each arm and between each leg.

As it can be seen in Figure 4-7, DSCC model is nonlinear. Even if the grid is balanced, DSCC model contains relatively complex internal dynamics leading to complex control structure. The overall control in balanced grid can be separated into 7 different parts as described in Figure 4-8.

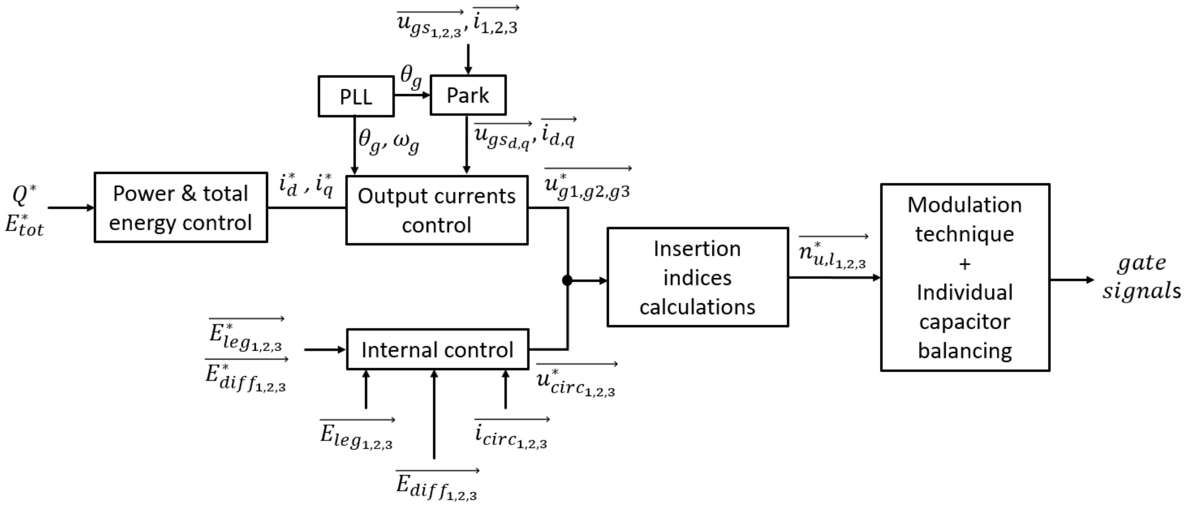

Figure 4-8: DSCC overall control block diagram in balanced grid

Reactive power reference and total energy reference are defined. The power & total energy controller defines output currents references. Then output current controllers give the output voltages references. In parallel, internal dynamic is controlled by following the leg energy and arm energy difference references. The internal control generates the circulating voltages references. Both output and circulating voltage references are used to calculate insertion indices references. Finally, a Phase-Shifted PWM (PS-PWM) modulation technique used in sub-modulation associated with a controller for balancing each individual capacitor create the gate signals to physically control the converter.

PLL and Park transformation are additional elements used respectively for converter synchronization with the grid and generation of grid voltage and current measurements in dq frame. These elements use standard techniques. This is why they are not developed in this report.

Except from the PLL and Park blocks, all the 5 other blocks in Figure 4-8 will be analysed in the next sections from the right to the left.

4.2.2 Modulation technique and individual capacitor balancing

As already mentioned, the PS-PWM modulation technique is used to convert the $\overrightarrow{n^*_{u,l_{1,2,3}}}$ into PWM signals to control each SM (inserting or bypassing them). This PWM generation technique is the best one concerning THD and help to maintain SM balancing in a leg. This leads to better internal dynamics management. The principle of the classical PS-PWM for upper arm of leg 1 is explained in Figure 4-9.

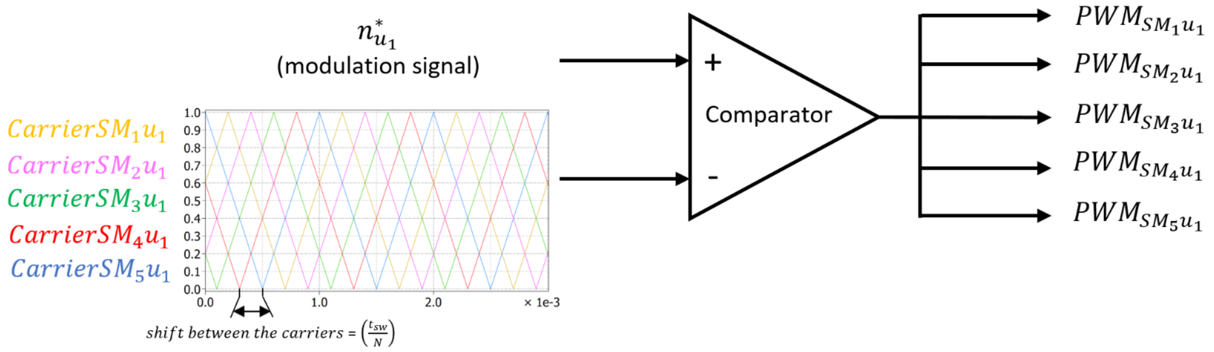

Figure 4-9: Classical PS-PWM principle for leg_1 upper arm with N = 5 submodules

Each carrier signal shifted equally over one period of commutation is compared with the arm insertion index reference. It generates a PWM signal for each SM of the arm. This PWM signal is sent to each gate driver which allows the insertion or bypass of the SM.

To improve the balancing of each capacitor voltage, N individual capacitor voltage balancing controllers are added in each arm. Each controller follows the principle shown in Figure 4-10.

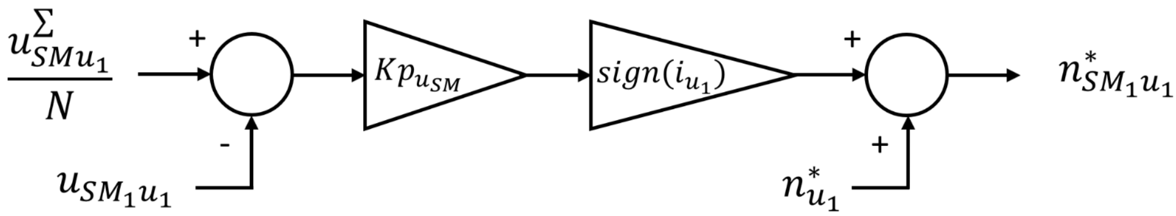

Figure 4-10: SM_1u_1 voltage balancing controller

The arm insertion index reference is slightly modified for each capacitor in one arm. Depending on the current direction in the arm, SM insertion index reference is slightly higher or lower than the arm insertion index reference. SM insertion index reference general equation is written in (3.26).

$$n^*_{SM_iu,l_{1,2,3}} = sign\left(i_{u,l_{1,2,3}}\right) \cdot K_{p_{u_{SM}}} \cdot \left(\frac{u^{\Sigma}_{SMu,l_{1,2,3}}}{N} - u_{SM_iu,l_{1,2,3}}\right) \quad (3.26)$$

Each $n^*_{SM_iu,l_{1,2,3}}$ is now a modulation signal reference for its related carrier signal. The principle of the proposed hybrid PS-PWM for leg_1 upper arm is shown in Figure 4-11.

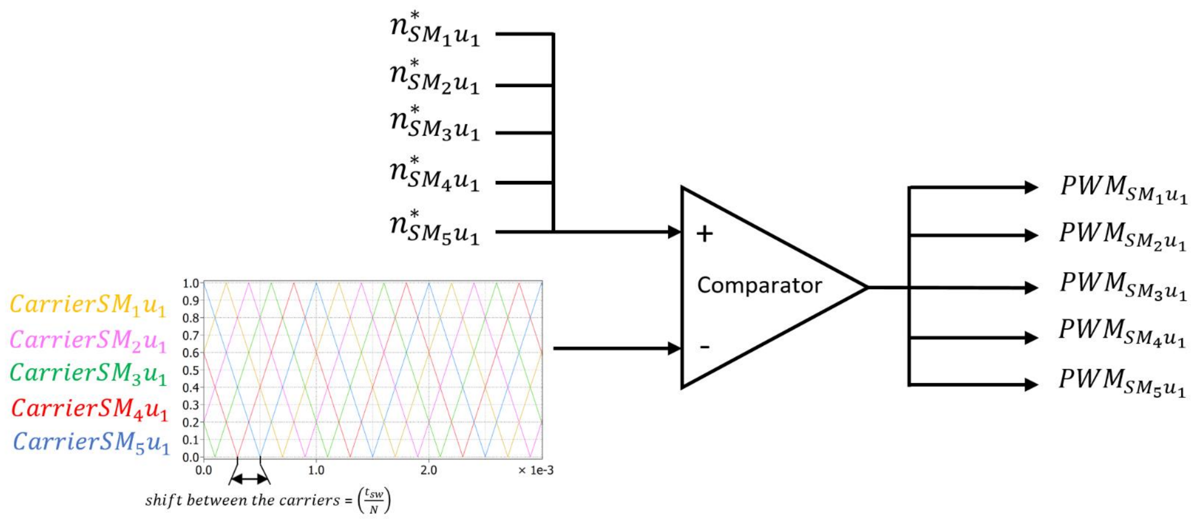

Figure 4-11: PS-PWM & individual capacitor balancing technique for leg_1 upper arm with N = 5 submodules

4.2.3 Arm insertion index references calculations

As it can be seen in Figure 4-7 and not considering the modulation, arm insertion index references are the inputs of the DSCC converter model. It means that insertion index references need to be calculated thanks to other variables which need to be controlled. In this section, a per phase analysis is realized for better reading.

As it can be seen in Figure 4-8, insertion index references are calculated thanks to u_g^* and u_{circ}^*.

Indeed, injecting (3.19) in (3.7), leads to (3.27).

$$\boxed{(3.7)\ \&\ (3.19)} \Rightarrow u_g = \frac{-u_u + u_l}{2} = \frac{-n_u \cdot u_{SMu}^{\Sigma} + n_l \cdot u_{SMl}^{\Sigma}}{2} \tag{3.27}$$

The same for circulating voltage, by injecting (3.19) in (3.11), leads to (3.28).

$$\boxed{(3.11)\&(3.19)(3.19)} \Rightarrow u_{circ} = \frac{u_u + u_l}{2} = \frac{n_u \cdot u_{SMu}^{\Sigma} + n_l \cdot u_{SMl}^{\Sigma}}{2} \tag{3.28}$$

By subtracting (3.27) to (3.28) and supposing the delay in voltage control negligible, n_u relationship (3.29) is obtained.

$$\boxed{(3.28) - (3.27)} \Rightarrow n_u = \frac{u_{circ} - u_g}{u_{SMu}^{\Sigma}} \approx \frac{u_{circ}^* - u_g^*}{u_{SMu}^{\Sigma}} \tag{3.29}$$

By adding (3.27) with (3.28) and supposing the delay in voltage control negligible, as for (3.29), n_l relationship (3.30) is obtained.

$$\boxed{(3.27) + (3.28)} \Rightarrow n_l = \frac{u_{circ} + u_g}{u_{SMl}^{\Sigma}} \approx \frac{u_{circ}^* + u_g^*}{u_{SMl}^{\Sigma}} \tag{3.30}$$

It is now possible to realize the block diagram of arm insertion index references calculations, shown in Figure 4-12.

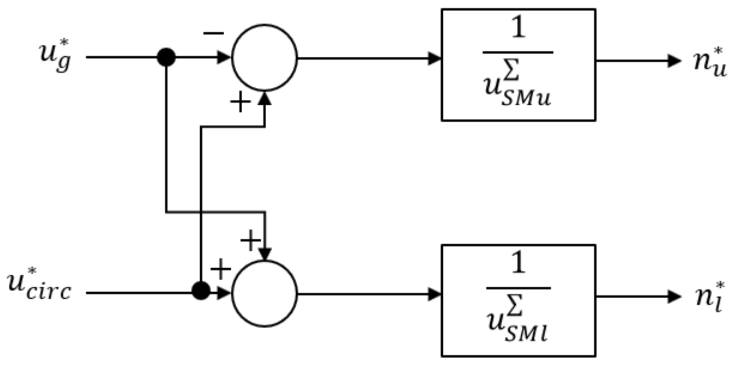

Figure 4-12: Arm insertion index references calculations block diagram

4.2.4 Output currents regulation

We now need to calculate the output voltages references $u_{g1,g2,g3}^*$. With the per phase schematic shown in Figure 4-12 and considering the DSCC block diagram in Figure 4-7, it is possible to generate u_g^* and u_{circ}^* references as proposed in Figure 4-13.

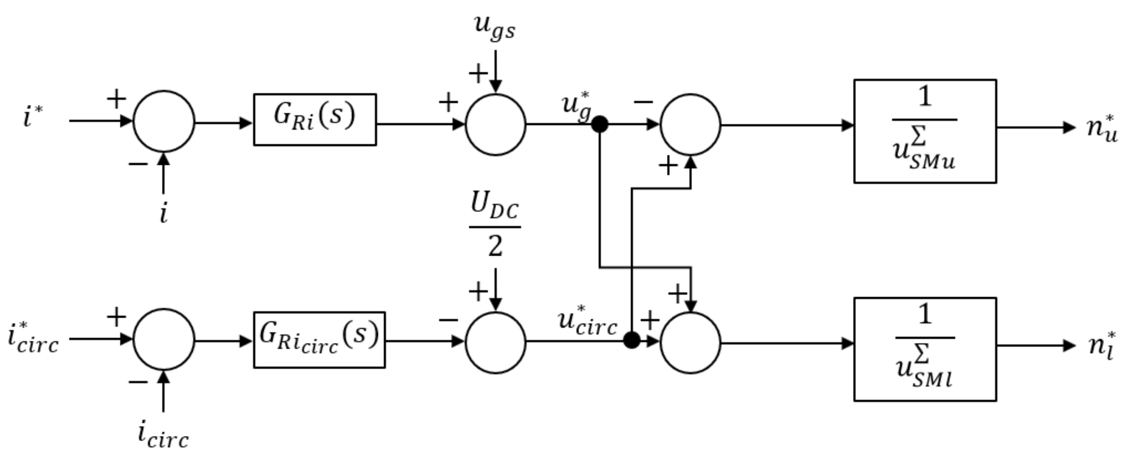

Figure 4-13: Per phase currents controller block diagram

There are 4 interesting points to underline in Figure 4-13:

- Output and circulating currents controls are separated.
- u_{gs}^* is added as a feed-forward used to counteract grid voltage.
- Output of the circulating current regulator is inversed considering the sign of circulating voltage in Figure 4-7.
- $\frac{U_{DC}}{2}$ is added as a feed-forward used for the same reason as from former point.

As already mentioned, output current control is realized independently from circulating current control. In this section, only output current control is presented. Furthermore, considering now the three phases, output currents references are generated using space vectors in dq frame. 3-phase output currents controller block diagram is shown in Figure 4-14.

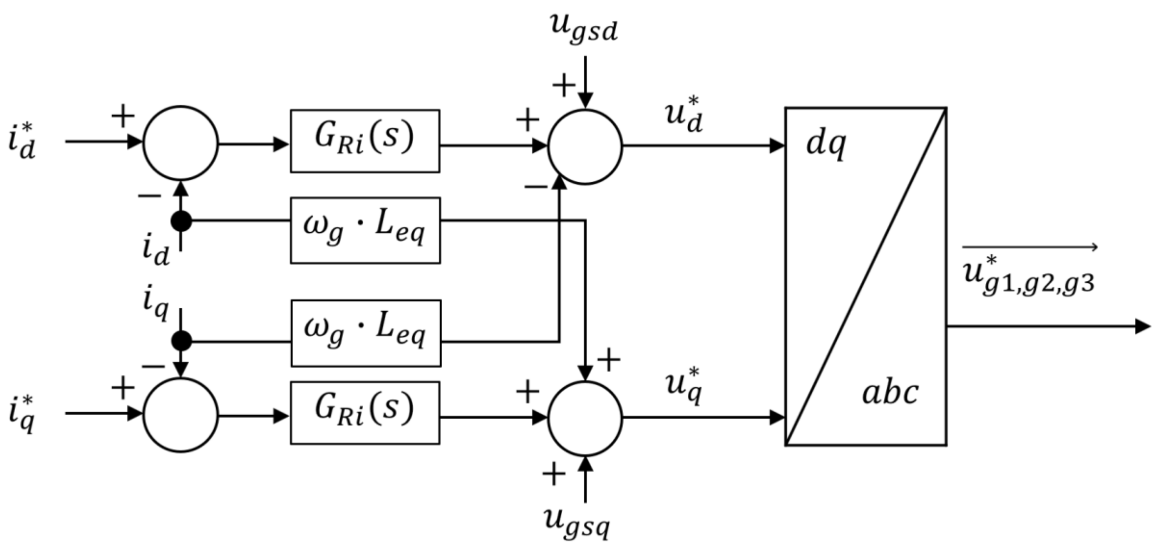

Figure 4-14: 3-phase output currents controller block diagram

L_{eq} is defined in (3.31) while ω_g is the grid angular frequency in [rad/s].

$$L_{eq} = \left(L_g + \frac{L_a}{2}\right) \tag{3.31}$$

Decoupling between i_d^* and i_q^* is realized. u_{gsd}^* and u_{gsq}^* are added as feed-forward, used to counteract grid voltage. As in Figure 4-13, after inverse Park transformation, output voltages references $u_{g1,g2,g3}^*$ are calculated and used in arm insertion index references calculation. PI controllers with same parameters are used for i_d^* and i_q^*.

4.2.5 Internal control

Internal control block, in combination with global energy control and individual capacitor balancing, maintain DSCC internal stability.

Internal control block diagram is shown in Figure 4-15.

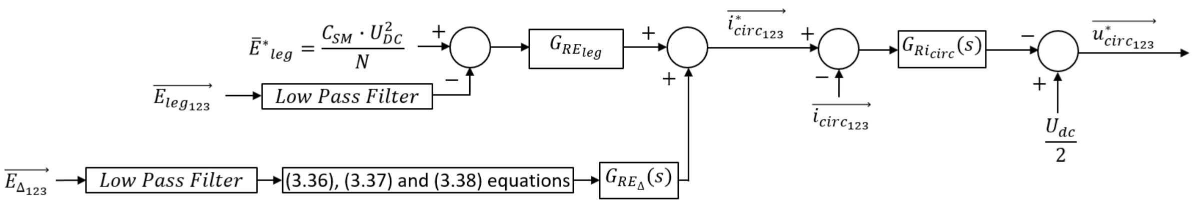

Figure 4-15 : Internal control block diagram

Internal control block is composed of 3 principal controllers:

- $\boldsymbol{G_{RE_{leg}}}$: Leg energy balancing controller which regulates the mean total energy in each leg to $\bar{E}^*{}_{leg} = \frac{C_{SM} \cdot U_{DC}^2}{N}$
- $\boldsymbol{G_{RE_\Delta}}$: Arm energy balancing controller which equals upper arm energy to lower arm energy in each leg.
- $\boldsymbol{G_{Ri_{circ}}}$: Circulating current controller which regulates the circulating current in each leg.

Furthermore, due to absence of physical DC-link, the sum of circulating current of each leg is zero as written in (3.32).

$$i_{circ_1} + i_{circ_2} + i_{circ_3} = 0 \tag{3.32}$$

The arm energy balancing controller ensures a balanced operation between the upper and lower arm by regulating the average energy stored in each of them at the same value. The arm energy difference is composed of a DC and a fundamental term. The fundamental component of the energy is directly linked with fundamental of the circulating current, which is responsible for exchanging active power between the converter's arms. The controller acts only on the fundamental component of the arm energy difference of each leg.

As already mentioned, circulating currents are coupled by nature in the DSCC. As a result, an injection of circulating current fundamental frequency in one arm of the DSCC leg would unavoidably couple with the other legs of the converter, if no further action is taken. According to [7], to achieve a decoupled control, injection of active current in one phase and reactive currents in the other phases is realized so that the average of the capacitor voltages is not shifted. Consequently, the total average energy difference remains unaffected. This concept leads to the following decoupling equations (3.33),(3.34) and (3.35), taken from [7].

$$i_{circ_1}^{1*} = \overline{E_{\Delta_1}(t)} \cdot \cos(\omega_1 \cdot t) + \frac{1}{\sqrt{3}}\overline{E_{\Delta_2}(t)} \cdot \cos(\omega_1 \cdot t + \frac{\pi}{2}) + \frac{1}{\sqrt{3}}\overline{E_{\Delta_3}(t)} \cdot \cos(\omega_1 \cdot t - \frac{\pi}{2}) \tag{3.33}$$

$$i_{circ_2}^{1*} = \overline{E_{\Delta_2}(t)} \cdot \cos(\omega_1 \cdot t - \frac{2\pi}{3}) + \frac{1}{\sqrt{3}}\overline{E_{\Delta_1}(t)} \cdot \cos(\omega_1 \cdot t - \frac{7\pi}{6}) + \frac{1}{\sqrt{3}}\overline{E_{\Delta_3}(t)} \cdot \cos(\omega_1 \cdot t - \frac{\pi}{6}) \tag{3.34}$$

$$i_{circ_3}^{1*} = \overline{E_{\Delta_3}(t)} \cdot \cos(\omega_1 \cdot t + \frac{2\pi}{3}) + \frac{1}{\sqrt{3}}\overline{E_{\Delta_1}(t)} \cdot \cos(\omega_1 \cdot t + \frac{7\pi}{6}) + \frac{1}{\sqrt{3}}\overline{E_{\Delta_2}(t)} \cdot \cos(\omega_1 \cdot t + \frac{\pi}{6}) \tag{3.35}$$

The complete principle of arm energy balancing controller works as follows. Energy measurements pass through the low pass filter with cutting frequency at $\frac{f_1}{10}$. Then the means are sent to the decoupled equations. It is worth to mention that this decoupling gives 3 signals at the fundamental frequency. These signals are the fundamental component refences for the circulating current in each leg and allow to maintain the balance of energy between arms in each leg.

The leg energy balancing controller maintains the average energy stored in each leg to a defined value given in (3.36).

$$\bar{E}^*{}_{leg} = \frac{C_{SM} \cdot U_{DC}^2}{N} \tag{3.36}$$

Indeed, as it can be seen in Figure 4-15, each leg energy is measured and passes through a low pass filter with cutting frequency at $\frac{2 \cdot f_1}{10}$ to access the mean value. The result is compared with the reference value $\bar{E}^*{}_{leg}$. The difference is regulated to zero by the $G_{RE_{leg}}$ regulator. The reference signal sent by this regulator represents the DC component of the circulating current for each leg.

The circulating current is regulated according to the reference values sent by the energy controllers above mentioned. As already expressed, the reference signal to follow is composed of a fundamental and DC component. Furthermore, the circulating current of an DSCC presents naturally a second order harmonic component when the current of fundamental frequency is controlled. To regulate properly all the frequency components of the circulating current, a Proportional Integral Resonant (PIR) controller $G_{Ri_{circ}}$ with control of fundamental and second harmonic component is used, as in [7].

Leg energy balancing controller is a proportional controller while arm energy balancing controller is a proportional controller with a sinusoidal component to generate the fundamental component setpoint for circulating currents.

4.2.6 Power and total energy control

As already mentioned, the purpose of the converter control is first to insure a control of reactive power injected in the PCC. This is why reactive power reference is required. Reactive power control is realized using the mathematical relationship between power and current in the dq frame. The general relationship is given by (3.37).

$$p + jq = \frac{3}{2} \cdot (U_d - jU_q) \cdot (I_d + jI_q) \tag{3.37}$$

Where:

- p is instantaneous active power [W]
- q is instantaneous reactive power [var]
- $(U_d - jU_q)$ is the conjugate of the voltage space vector in dq rotating frame at grid frequency
- $(I_d + jI_q)$ is the current space vector in dq rotating frame at grid frequency

Isolating the real and imaginary part of the right-hand side of (3.37) leads to (3.38) and (3.39).

$$p = \frac{3}{2} \cdot (U_d \cdot I_d + U_q \cdot I_q) \tag{3.38}$$

$$q = \frac{3}{2} \cdot (U_d \cdot I_q - U_q \cdot I_d) \tag{3.39}$$

Using a PLL synchronized on the grid frequency to set the parameter U_q to zero leads to (3.40) and (3.41).

$$p = \frac{3}{2} \cdot U_d \cdot I_d \tag{3.40}$$

$$q = \frac{3}{2} \cdot U_d \cdot I_q \tag{3.41}$$

Thanks to (3.41), the relationship between Q^* and i_q^* is available. Remastering (3.41) putting I_q as a function of q, it is now possible to generate i_q^* setpoint based on the desired Q^*. It is given in (3.42).

$$i_q^* = Q^* \cdot \frac{2}{3 \cdot U_d} \tag{3.42}$$

As shown from (3.40), i_d^* setpoint is responsible of active power exchange between the converter and the grid. In STATCOM application, ideally no active power is exchanged. However, in practice, active power is exchanged to cover the converter losses. The losses are not constant over the time. It means that a controller has to be set to calculate the real time amount of active power to absorb from or inject in the grid. This controller is realized by controlling the real time total energy stored in the DSCC at a constant desired value. It allows the DSCC to have the total energy needed to maintain the internal dynamics in a stable operation. Furthermore, in steady state conditions, it regulates $\bar{U}_{PN}$ to U_{DC} (where U_{DC} is the setpoint needed to satisfy the DSCC mathematical modelling exposed above). Indeed, the total energy stored in the DSCC is the sum of the 3 leg energies which are regulated as reminded in (3.43).

$$\bar{E}^*{}_{leg} = \frac{C_{SM} \cdot U_{DC}^2}{N} \tag{3.43}$$

It leads to a total energy setpoint E_{tot}^* in the DSCC given in (3.44).

$$E_{tot}^* = 3 \cdot \bar{E}^*{}_{leg} = 3 \cdot \frac{C_{SM} \cdot U_{DC}^2}{N} \tag{3.44}$$

C_{SM} and N are constant values. Considering that $\bar{E}^*{}_{leg} = \bar{E}_{leg}$ for each phase, means that $E_{tot} = E_{tot}^*$ and finally $U_{DC} = \bar{U}_{PN}$. A PI controller is used to control the total energy of the converter.

Figure 4-16 shows power and total energy control block diagram.

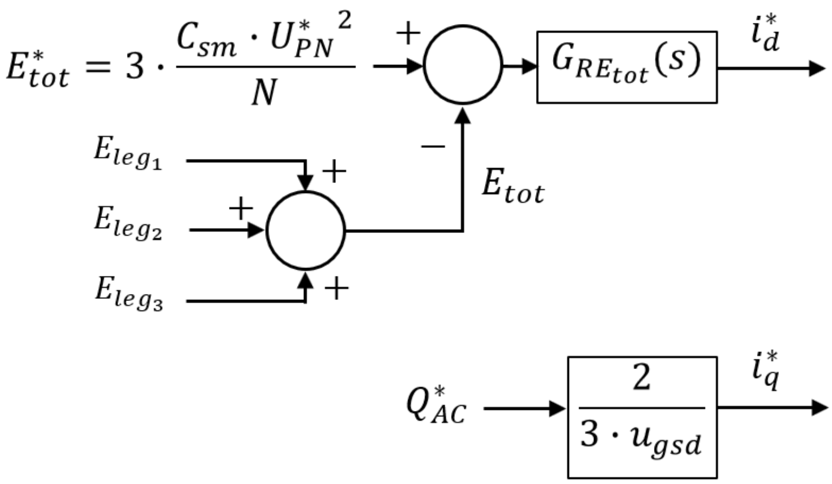

Figure 4-16: Power and total energy control block diagram

This last figure completes the description of the DSCC control in balanced grid.

4.3 Control in unbalanced grid

The DSCC control in balanced grid is not sufficient when the grid becomes unbalanced. It leads to grid desynchronization and internal divergence of arm voltages. These issues are not acceptable when connected to the grid in case of unbalanced. This is why a second control scheme is proposed.

4.3.1 Overall control in unbalanced grid

To deal with unbalanced grid, the new overall diagram is given in Figure 4-17.

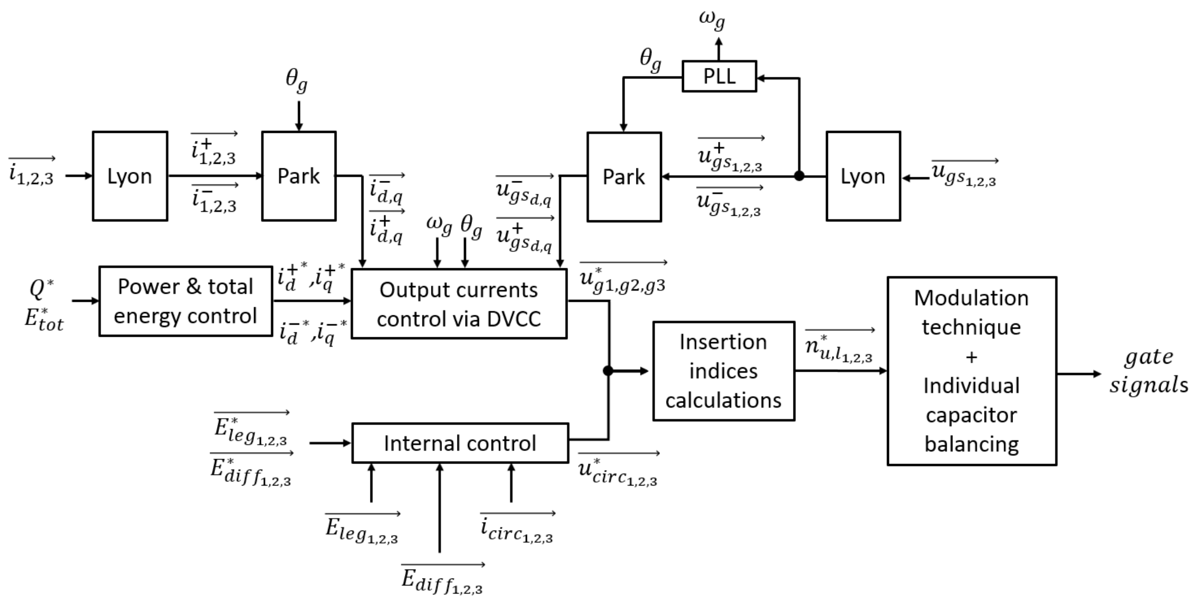

Figure 4-17: DSCC overall control block diagram in unbalanced grid

It changes a bit the overall control presented in Figure 4-8. As for SSBC in unbalanced grid conditions, output voltage references $\overrightarrow{u_{g1,g2,g3}^*}$ are calculated using PLL, Lyon and Park transformations as presented in section 162.6. Internal control block, as well as the insertion indices calculations and gate signal generation blocks are the same blocks used in the balanced control. In the next sections, only the new blocks are presented.

4.3.2 DVCC for DSCC

The DVCC block detailed in Figure 4-18 contains the current regulators for the dq currents of the positive and negative sequence. The outputs of the current controllers pass through the inverse Park transformation and are summed to give the final output voltage references $\overrightarrow{u^*_{g1,g2,g3}}$. This decoupling between the positive and negative sequences allows to control individually the two sequences. The principle is the same as the one of the SSBC and SDBC topologies.

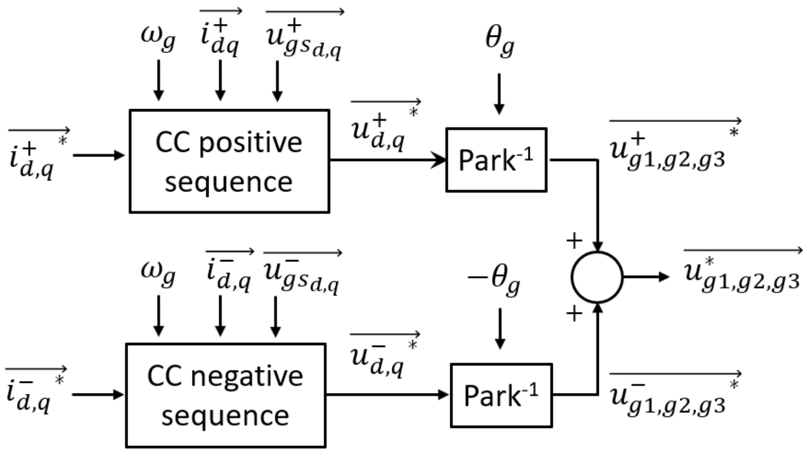

Figure 4-18: DVCC block diagram for DSCC

Here the CC positive and negative sequences are using the principle shown in Figure 4-14 replacing dq components by either the positive or the negative corresponding sequence.

4.3.3 Power and total energy control in unbalanced grid

The total energy control is still the same but this time, it generates the i_d^{+*}reference. i_q^{+*} is now the output of the power calculations in dq frame for Q^* using $u^+_{gs_d}$. It is important to note that during grid unbalanced, $u^+_{gs_d}$ is smaller than u_{gs_d} in balanced grid. It means that i_q^{+*} has to be limited not to exceed the maximum power of the STATCOM. Figure 4-19 shows the equivalent block diagram.

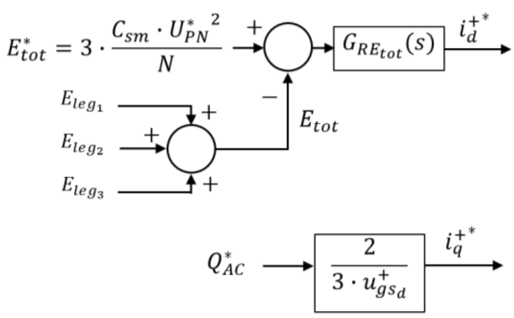

Figure 4-19: Power and total energy control block diagram in unbalanced grid

5 OPERATING RANGE OF THE PROJECT

The operating range in this project is well defined. From [1], we know that the current exchanged between the STATCOM and the grid is balanced. Furthermore, the grid voltage has a low level of unbalance in normal operation but can also have a high degree of unbalance ($\hat{U}_n/\hat{U}_p$) if a fault occurs in the grid. The objective is that the STATCOM continue to operate even during the fault condition.

In [1], the different faults occurring in the grid are analysed. The results are summarized in the Table 5-1.

Substation	Boisdavaux				Polny			
sc type	**single-phase**		**two-phase**		**single-phase**		**two-phase**	
	Amplitude [pu]	Phase [rad]	amplitude [pu]	phase [rad]	amplitude [pu]	phase [rad]	amplitude [pu]	phase [rad]
U_p	0.986	2.624	0.492	-2.094	0.987	-2.211	0.640	-0.259
U_n	0.006	2.405	0.492	2.094	0.005	-2.524	0.352	-2.213
U_0	0.992	-0.519	0.492	0.000	0.996	0.923	0.493	1.915

Table 5-1 : Grid voltage at "Boisdavaux" substation sequences when a fault occurs in the grid

The grid defaults are a single-phase or a two-phase to earth short-circuit. These defaults could appear at the "Boisdavaux" or "Polny" substations. When the fault occurred, the temporal voltages at the PCC of the STATCOM are simulated and transformed in the positive, negative and zero sequences. Their amplitude are expressed in per unit and the phase in radian gives the phase of the phasor A. Obviously, the phasors B and C have a phase difference of ±2π/3 with the phasor A. Finally, the zero sequence voltage are in phase for the A, B and C phasors.

From the results presented in the Table 5-1, three cases can be defined:

1. Single-phase short-circuit: no matter in which substation the default occurs, the positive and zero sequences are near 1 pu and the negative sequence is near 0 pu.
2. Two-phase short-circuit in Boisdavaux: the three sequences have the same amplitude. It gives a high degree of unbalance U_n/U_p= 1.
3. Two-phase short-circuit in Polny: the three sequences have different amplitude. The degree of unbalance is smaller than in the previous case, U_n/U_p= 0.55.

One important thing which is the same in the three cases is that the zero sequence in the grid voltages will not be seen by the STATCOM. Indeed, because the STATCOM is not referenced (linked) to the neutral line of the grid, the system can be considered as floating and thus it will not be affected by the zero sequence voltage of the grid.

Concerning the current exchanged between the STATCOM and the grid, it is supposed that it is balanced in each case. The amplitude is equal to 1 pu and the majority is given by the reactive power (90° phase-shift current compared to the PCC voltage). A little amount of the current is given by the active power (in phase current) to compensate the losses in the STATCOM.

Each STATCOM topology work well on a balanced grid without any fault. So, the effectiveness evaluation of each STATCOM topology is done on its capability to operate properly when a fault occurs in the grid. The three STATCOM structures are evaluated here under:

- **SSBC**: as explain in the section 2.6.1.1, the ZSVC strategy control is sensitive to the degree of current unbalance I_n/I_p and support well unbalanced voltage. The Figure 2-15 shows that if I_n/I_p = 1, the zero sequence voltage to generate tends to infinity. But, as explained above, the currents are well balanced, thus the ZSVC strategy seems to be a good solution for the different operating points. On the contrary, the NSCC strategy cannot be used when it has a two-phase short-circuit at the substation "Boisdavaux" because U_n/U_p= 1 (see explication in the section 2.6.2).
- **SDBC**: as explain in the section 3.3.1.1**Erreur ! Source du renvoi introuvable.**, the ZSCC strategy control is sensitive to the degree of voltage unbalance U_n/U_p and support well unbalanced current. The Figure 3-7 shows that if U_n/U_p = 1, the zero sequence current to generate tends to infinity. This degree of voltage unbalance U_n/U_p = 1 is reach when it has a two-phase short-circuit at the substation "Boisdavaux". Due to this, the ZSCC strategy cannot

be used at this operating point. It is the same conclusion for the NSCC strategy as explain in the SSBC structure.

- **DSCC**: According to state of the art presented in [1], DSCC topology, having more degree of freedom than SSBC and SDBC and with a suitable control, is able to work with every type of unbalance. The single-phase short-circuit is managed correctly with the control proposed in section 4.3 (verified by simulations). However for two-phase short-circuit, in the literature, this control has never been tested and in the current state of the simulation analyses, it appears that DSCC internal dynamics is not stable for all types of reactive power exchanged. To verify this case, an entire operating range of the DSCC was not found in the literature and has to be calculated. HEIG-VD team needs more time to realize this study and draw a conclusion on this case.

As a conclusion, from the analysis here above, the SSBC topology with the ZSVC strategy is selected for the simulation analysis because it seems to work well in all the operating points of the project. On the contrary, the SDBC structure will not be more simulated because it was demonstrated that it cannot work in the case of a two-phase short-circuit at the “Boisdavaux” substation.

For the DSCC, the question is still open and need further investigations. An additional report presenting the results will be sent later on.

6 SIMULATION RESULTS

In the previous chapters (2, 3 and 4), three topologies were presented and analysed. They are the SSBC, the SDBC and the DSCC. Furthermore, in the chapter 5, the operating range of the project, and in particular when a fault occurs in the grid, shows that the SDBC cannot works properly in all operating points of the project. So, only the SSBC and the DSCC will be simulated in more details. The simulations are done in the simulation software PLECS.

For each STATCOM structure, the first part of simulations proves the well operation of the system on a balanced grid with unbalanced cluster voltages $u^{\Sigma}_{SM_L}$ (for SSBC) or $u^{\Sigma}_{SMu,l}$ (for DSCC). The control strategy must rebalance the cluster voltages when it is activated.

The second part of simulations proves the well operation of the STATCOM in case of an unbalanced system due to a fault in the grid. The three possible operating points with a fault in the grid are defined in the chapter 0.

6.1 SSBC SIMULATIONS

As a reminder, the Figure 2-1 represents the schematic of the converter. The simulation parameters are defined in the Table 6-1.

Parameter	Value	Parameter	Value
U_{gs}	400/√3 [V]	C_{sm}	3.63 [mF]
f_g	50 [Hz]	S_{1pu}	5 [kVA]
L_g	10 [µH]	$u^{\Sigma}_{SM_L}$	425 [V]
R_g	10 [mΩ]	f_{sw}	1 [kHz]
L_a	15 [mH]	$t_{deadband}$	1 [µs]
R_a	200 [mΩ]	f_{sample}	5 [kHz]
N_{sm}	5 [-]		

Table 6-1 : simulation parameters for the SSBC simulations

S_{1pu} is the nominal apparent power of the converter. $u^{\Sigma}_{SM_L}$ is the nominal value for the cluster voltage. Each submodule switch at a frequency of f_{sw} with a dead-band time of $t_{deadband}$. Finally, the sampling of each measure is done at f_{sample} ($f_{sw} \cdot N_{sm}$).

6.1.1 Rebalancing of the cluster voltage

In this simulation, the STATCOM exchanges the nominal reactive power with positive sequence current. At the beginning, the ZSVC control strategy is deactivated. At 0.2 [s], a negative sequence current is generates to unbalance the cluster voltages $u^{\Sigma}_{SM_L}$. At 0.25 [s], the negative sequence current is removed and it remains only the positive sequence. Finally, at 0.3 [s], the ZSVC control strategy is activated. The Figure 6-1 shows the more interesting quantities of the simulation.

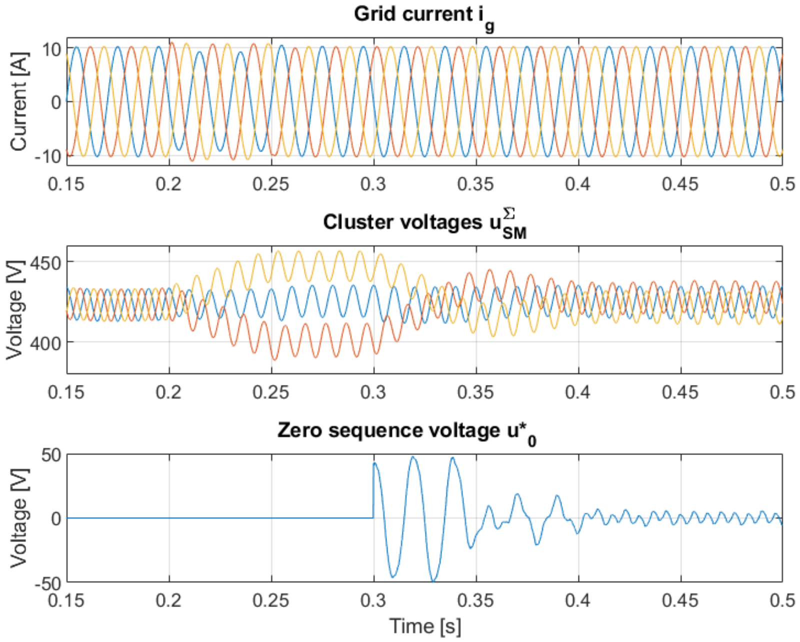

Figure 6-1 : SSBC, rebalancing of the cluster voltage simulation

Each part of time is analysed here below. Keep in mind that the voltage at the PCC are balanced during all this simulation:

- 0.15 [s] < t < 0.2 [s]: the grid currents are balanced and so the cluster voltages remain well balanced.
- 0.2 [s] < t < 0.25 [s]: the grid currents are unbalanced, because the ZSVC control strategy is not activated, the cluster voltages derived from their stable average value.
- 0.25 [s] < t < 0.3 [s]: the grid currents are balanced again. The cluster voltages stay at their unbalanced values.
- 0.3 [s] < t < 0.5 [s]: the ZSVC control strategy is activated as it is visible on the last graph ($u_0^* \neq 0$). The cluster voltages present a transient and are rebalanced.

Note that the currents grid have a THD of 0.4% at 0.5 [s]. This THD increase only of 0.1% when the cluster voltages are unbalanced and the ZSVC is activated.

This simulation demonstrates that when the grid voltage at the PCC are balanced and the cluster voltages are unbalanced, the ZSVC is able to rebalance the cluster voltages thanks to the generation of the zero sequence voltage.

6.1.2 One-phase short-circuit

Now, it is checked that the STATCOM is able to continue to operate when a one-phase short-circuit occurs in the grid. As explain in the chapter 5, wherever the short-circuit appears, the PCC voltages seen by the STATCOM is quiet the same.

In this simulation, the STATCOM exchanges the nominal reactive power with positive sequence current before the fault occurs. Once the fault appears at 0.2033 [s], the objective of the converter is to continue to exchange the same amount of current as before the fault apparition. The Figure 6-2 shows the more interesting quantities of the simulation.

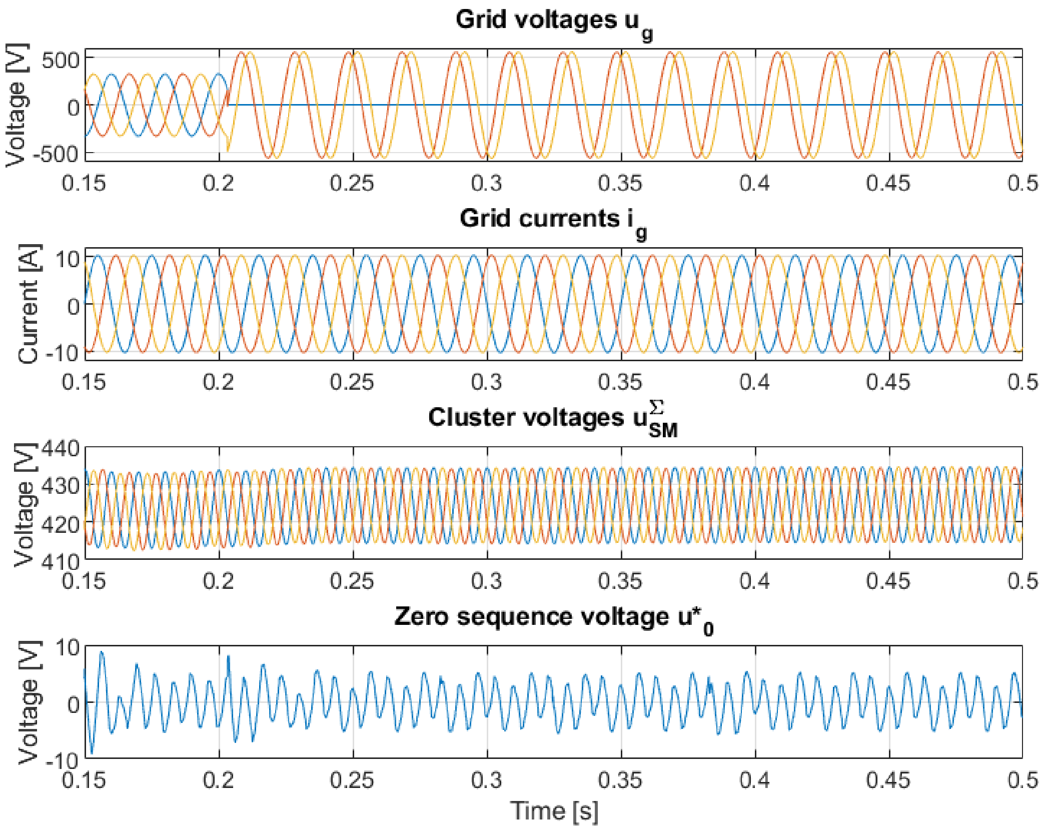

Figure 6-2 : SSBC, one-phase short-circuit simulation

The grid currents and the cluster voltages do not change between before and after the default apparition. More, the ZSVC control strategy does not seem to change its behaviour when the fault occurs. As explain in the chapter **Erreur ! Source du renvoi introuvable.** , this is because the converter is not influenced by the zero sequence voltage of the grid. So it sees only the positive sequence and a very little negative sequence voltage. Note that if the ZSVC control strategy is removed, the little amount of negative sequence voltage will drift softly the cluster voltages $u^{\Sigma}_{SM_{Li}}$. So the ZSVC control strategy must be implemented to have a good operation of the converter. Finally, the grid currents present, as the previous point, a THD of 0.4%.

6.1.3 Two-phase short-circuit

In this section, it is checked that the STATCOM is able to continue to operate when a two-phase short-circuit occurs in the grid. From the chapter 5, it has two interesting substations where the short-circuit is done. Boisdavaux and Polny.

In this simulation, the STATCOM exchanges the nominal reactive power with positive sequence current before the fault occurs. Once the fault appears at 0.2033 [s], the objective of the converter is to continue to exchange the same amount of current as before the fault apparition. The Figure 6-3 shows the more interesting quantities of the simulation for the short-circuit at Boisdavaux substation.

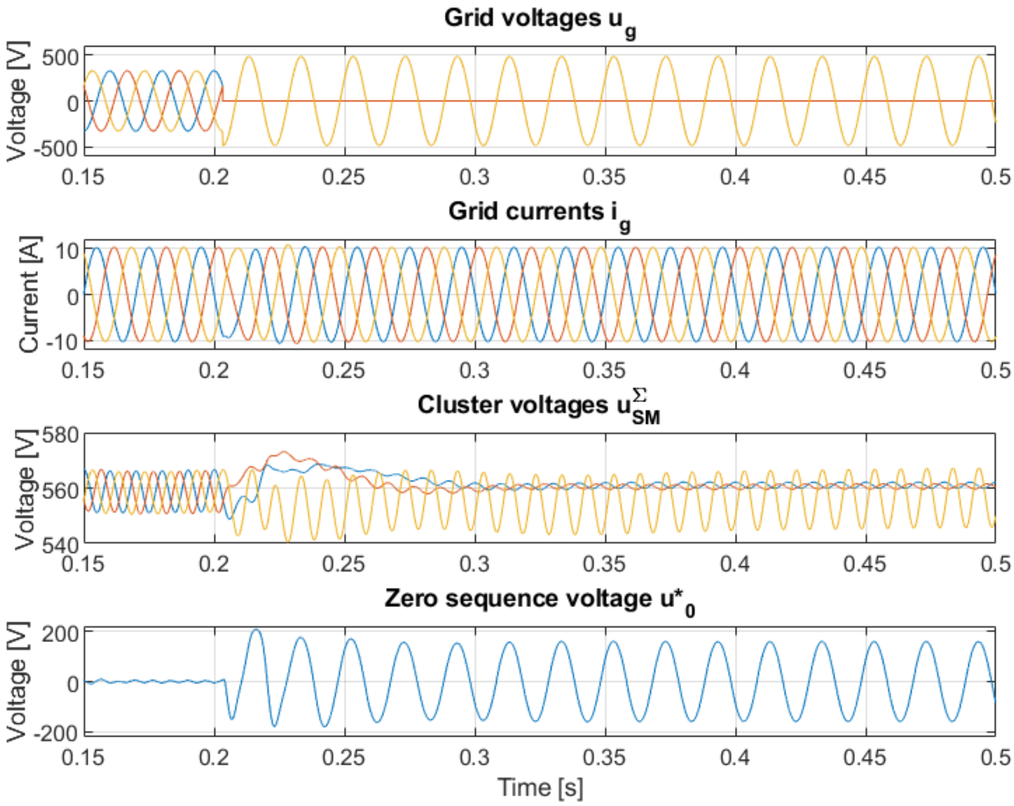

Figure 6-3 : SSBC, two-phase short-circuit at Boisdavaux simulation

It is important to note that the cluster voltages $u^{\Sigma}_{SM_{Li}}$ had to be increased in order to be able to generate the zero sequence voltage with a high amplitude (about 200 [V]). So, the average cluster voltages were increased from 425 [V] to 560 [V] (+32%).

When the fault appears, the ZSVC control strategy generates a zero sequence voltage about 200 [V] amplitude. The control makes possible to limit the unbalance of the cluster voltage and even to rebalance them. If the ZSVC control strategy is removed, the cluster voltages reached quickly the physical values for a well operation of the converter. Finally, the grid currents present a THD of 0.6%. Compare to the previous section, this is half more and is due to the increase of the cluster voltage which allow to generate larger output voltage but with a lower resolution since the number of cells has not changed (N_{SM} = 5).

The Figure 6-4 shows the results of the simulation for the short-circuit at Polny substation. Here, the same analysis can be done as for the short-circuit at Boisdavaux substation. It can ben noted that the zero sequence voltage amplitude is lower than for two-phase short-circuit at Boisdavaux. The short-circuit in Polny is then less critical than the one directly at the Boisdavaux substation.

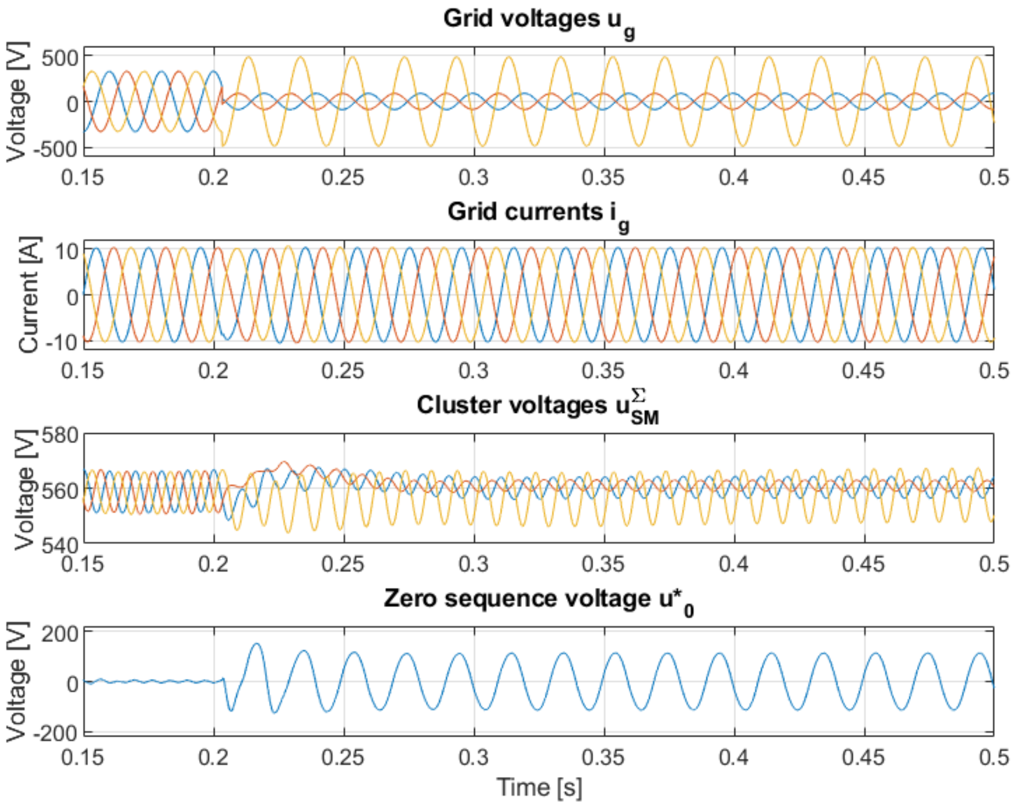

Figure 6-4 : SSBC, two-phase short-circuit at Polny simulation

6.2 DSCC SIMULATIONS

As a reminder, the Figure 4-1 represents the schematic of the converter. The simulation parameters are defined in the Table 6-2.

Parameter	Value	Parameter	Value
U_{gs}	$400/\sqrt{3}$ [V]	C_{sm}	3.3 [mF]
f_g	50 [Hz]	S_{1pu}	5 [kVA]
L_g	3 [mH]	$u_{SM_{u,l}}^{\Sigma}$	800 [V]
R_g	100 [mΩ]	f_{sw}	1 [kHz]
L_a	6 [mH]	$t_{deadband}$	1 [µs]
R_a	200 [mΩ]	f_{sample}	5 [kHz]
N_{sm}	5 [-] (by arm)		

Table 6-2 : simulation parameters for the SSBC simulations

S_{1pu} is the nominal apparent power of the converter. $u_{SM_{u,l}}^{\Sigma}$ is the nominal value for the cluster voltage (by arm). Each submodule switch at a frequency of f_{sw} with a dead-band time of $t_{deadband}$. Finally, the sampling of each measure is done at f_{sample} ($f_{sw} \cdot N_{sm}$), as for the SSBC.

6.2.1 Rebalancing of the internal voltages

In this simulation, the STATCOM exchanges the nominal reactive power with positive sequence current. Before 0.4 [s], overall DSCC control is activated. At 0.4 [s], a negative sequence current is generated and internal as well as total energy controllers are deactivated to unbalance the leg cluster voltages $u_{SM_{Leg}}^{\Sigma}$ and the arm cluster voltages $u_{SM_u}^{\Sigma}$ and $u_{SM_l}^{\Sigma}$ within one leg. At 0.45 [s], the negative sequence current is removed and it remains only the positive sequence. Finally, at 0.5 [s], the overall control is activated. The Figure 6-5 shows the more interesting quantities of the simulation.

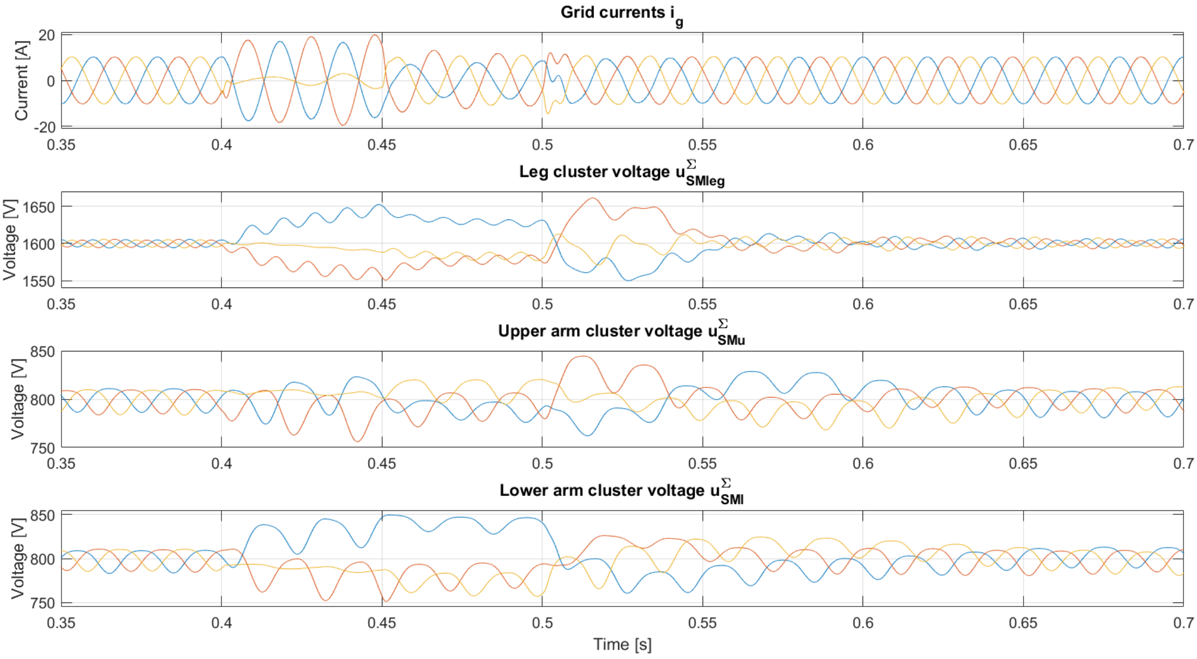

Figure 6-5: DSCC rebalancing of internal voltages simulation

Each part of time is analysed here below. Keep in mind that the voltage at the PCC are balanced during all this simulation:

- 0.35 [s] < t < 0.4 [s]: the grid currents are balanced and so all the internal cluster voltages remain well balanced (thanks to internal control).
- 0.4 [s] < t < 0.45 [s]: the grid currents are unbalanced and because the internal controls are not activated, the leg and arm cluster voltages derived from their stable average value (each one in a different way). It can be seen that $u^{\Sigma}_{SM_{u1}}$ (in blue) arm cluster voltage and thus the $u^{\Sigma}_{SM_{leg1}}$ (in blue) leg cluster voltage are the most affected.
- 0.45 [s] < t < 0.5 [s]: the grid currents are balanced again without the internal controls. The cluster voltages stay globally at their unbalanced values.
- 0.5 [s] < t < 0.7 [s]: all internal controls are activated. The leg and arm cluster voltages present a transient and are rebalanced.

Note that the grid currents have a THD of 0.9 [%] at 0.7 [s]. This THD is 1.2% higher during the rebalance at 0.55 [s]. This is also a good THD given that this case is a case that shouldn't appear in reality. Indeed, internal controls are always activated preventing this kind of internal unbalance.

This simulation demonstrates that when the grid voltage at the PCC are balanced and the cluster voltages are unbalanced, the internal control is able to rebalance the cluster voltages.

6.2.2 One-phase short-circuit

Now, it is checked that the DSCC is able to continue to operate when a one-phase short-circuit occurs in the grid. As already explained in the previous chapters, wherever the short-circuit appears, the PCC voltages see by the STATCOM is quiet the same.

In this simulation, the DSCC exchanges the nominal reactive power with positive sequence current before the fault occurs. Once the fault appears at 0.3888 [s], the objective of the converter is to continue to exchange the same amount of current as before the fault apparition. The Figure 6-6 shows the more interesting quantities of the simulation

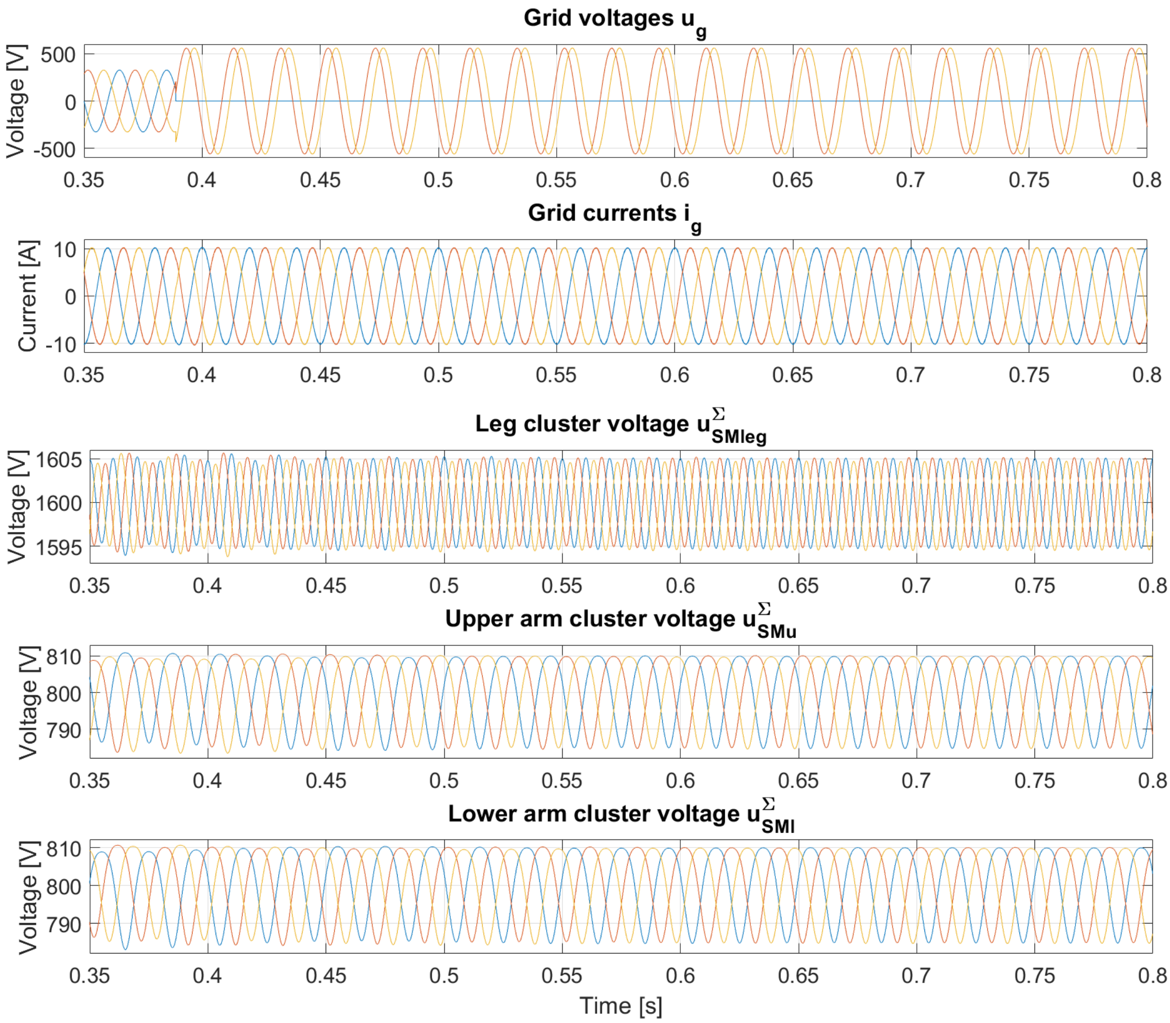

Figure 6-6: DSCC one-phase short-circuit simulation results

The grid currents and the internal cluster voltages stay the same before and after the default apparition. Even during the short circuit (here during 0.4 [s]), the right amount of current is exchanged and the internal cluster voltages stay balanced around the nominal value. It validates the correct operation of DSCC during one-phase short-circuit in the grid. As explained for the SSBC, this is because the converter is not influenced by the zero sequence voltage of the grid. It sees only the positive sequence and a very little negative sequence voltage. To confirm the results, THD before and after is measured. Grid currents THD is 0.9 [%] at t = 0.35 [s] and 1.0 [%] at t = 0.7 [s]. THD is not affected during the short-circuit.

6.2.3 Two-phase short-circuit

This section does not contain any simulation results because these results are not conclusive.

As mentioned in the section 5, according to state of the art presented in [1], DSCC topology has more degree of freedom than SSBC and SDBC. Therefore, with a suitable control, DSCC should be able to work with every type of unbalance. However, for two-phase short-circuit, in the current state of the simulation analyses, it appears that DSCC internal dynamics is not stable and internal cluster voltages drift until impossible values. As a consequence, grid current exchanged is also greatly distorted with a THD of around 20%. All these elements are not acceptable.

In order to see if this control and topology are able to work in such default case, the entire operating range of the DSCC has to be calculated in the same way as for other topologies. No information for this was found in the literature. HEIG-VD team needs more time to realize this study and draw a conclusion on this case. Another report will be provided later on to present the results of this part.

7 CONCLUSION

This report presents the theory analysis of three different converter topologies: the SSBC, the SDBC and the DSCC. The operating range of each topology was studied. In parallel, several operating points of the grid in this project were taken from the analysis done in [1]. By comparing the different operating range/points, the SDBC topology has been removed from the potential solutions since it cannot operate properly when the condition U_n/U_p = 1 is reached. This condition of large degree of unbalance of the grid voltage can appear when it has a two-phase short-circuit.

Finally, the SSBC topology with the ZSVC strategy has demonstrated that the converter is able to continue to operate even when a one-phase or a two-phase short-circuit occurs in the grid. It was proven that the currents continue to be generated with a low THD and that the cluster voltages stay balanced thanks to the ZSVC control strategy.

Concerning DSCC topology control strategy presented, results are conclusive for one-phase short-circuits appearing in the grid. However, additional time is needed to analyse more in details if two-phase short-circuit are possible to manage with this topology and control. Another report will be provided later on to present the results of this part.

8 BIBLIOGRAPHIE

[1] G. Grosjean, G. Courteau, S. Kissling, M. Bozorg and M. Carpita, “D1.1 - Report on Modular STATCOM structures: Comparaison des structures,” COSTAM Deliverable, Yverdon-les-Bains, Switzerland, 2021.

[2] C. L. Fortescue, “Method of Symmetrical Coordinates Applied to the Solution of Polyphase Networks,” *Transactions of the AIEE,* vol. II, no. 37, pp. 1027-1140, 1918.

[3] R. Teodorescu, M. Liserre and P. Rodríguez, Grid Converters for Photovoltaic and Wind Power Systems, John Wiley & Sons, Ltd. ISBN: 978-0-470-05751-3, 2011.

[4] R. Betz and T. Summers, “Introduction to symmetrical components and their use in statcom applications,” University of Newcastle, Australia, School of Electrical Engineering and Computer Science, November 2009.

[5] Lyon and W. V., Application of the Method of Symmetrical Components, New York: McGraw-Hill, 1937.

[6] E. Behrouzian, “On control of cascaded H-bridge converters for STATCOM applications,” Chalmers university of technology, Gothenburg, Sweden, 2017.

[7] G. Tsolaridis, E. Kontos, S. K. Chaudhary, P. Bauer and R. Teodorescu, “Internal balance during low-voltage-ride-through of the modular multilevel converter STATCOM,” *Energies, vol. 10, n°7,* 2017, doi: 10.3390/en10070935.

9 APPENDIX

9.1 ZSVC DEVELOPMENT

Let assume that all the quantities are sinusoidal. The SSBC will generate positive, negative and zero sequences arm voltages $\overrightarrow{u_{SM_{Li}}}$. These definitions are shown in the equations (9.1).

$$
\begin{aligned}
\underline{I}_{L_1} &= \hat{I}_p \cdot e^{j\cdot\delta_p} + \hat{I}_n \cdot e^{j\cdot\delta_n} \\
\underline{I}_{L_2} &= \hat{I}_p \cdot e^{j\cdot\left(\delta_p - \frac{2\cdot\pi}{3}\right)} + \hat{I}_n \cdot e^{j\cdot\left(\delta_n + \frac{2\cdot\pi}{3}\right)} \\
\underline{I}_{L_3} &= \hat{I}_p \cdot e^{j\cdot\left(\delta_p + \frac{2\cdot\pi}{3}\right)} + \hat{I}_n \cdot e^{j\cdot\left(\delta_n - \frac{2\cdot\pi}{3}\right)} \\
\underline{U}_{SML1} &= \widehat{U}_p \cdot e^{j\cdot\theta_p} + \widehat{U}_n \cdot e^{j\cdot\theta_n} + \widehat{U}_0 \cdot e^{j\cdot\alpha_0} \\
\underline{U}_{SML2} &= \widehat{U}_p \cdot e^{j\cdot\left(\theta_p - \frac{2\cdot\pi}{3}\right)} + \widehat{U}_n \cdot e^{j\cdot\left(\theta_n + \frac{2\cdot\pi}{3}\right)} + \widehat{U}_0 \cdot e^{j\cdot\alpha_0} \\
\underline{U}_{SML3} &= \widehat{U}_p \cdot e^{j\cdot\left(\theta_p + \frac{2\cdot\pi}{3}\right)} + \widehat{U}_n \cdot e^{j\cdot\left(\theta_n - \frac{2\cdot\pi}{3}\right)} + \widehat{U}_0 \cdot e^{j\cdot\alpha_0}
\end{aligned}
\tag{9.1}
$$

The active power in each phase can be calculated by:

$$
P_{L_i} = \Re\{\underline{S}_{L_i}\} = \Re\{\underline{U}_{SML_i} \cdot \underline{I}^*_{L_i}\} = P_{com} + P_{imb\,Li} \tag{9.2}
$$

with:

$$
P_{com} = \frac{\widehat{U}_p \cdot \hat{I}_p}{2} \cdot cos(\theta_p - \delta_p) + \frac{\widehat{U}_n \cdot \hat{I}_n}{2} \cdot cos(\theta_n - \delta_n) = \frac{P_{3\Phi}}{3} \tag{9.3}
$$

and

$$
\begin{aligned}
P_{imb\,L1} &= \underbrace{\frac{\widehat{U}_p \cdot \hat{I}_n}{2} \cdot cos(\theta_p - \delta_n) + \frac{\widehat{U}_n \cdot \hat{I}_p}{2} \cdot cos(\theta_n - \delta_p)}_{K_1} + \frac{\widehat{U}_0 \cdot \hat{I}_n}{2} \cdot cos(\alpha_0 - \delta_n) \\
&\quad + \frac{\widehat{U}_0 \cdot \hat{I}_p}{2} \cdot cos(\alpha_0 - \delta_p) \\
P_{imb\,L2} &= \underbrace{\frac{\widehat{U}_p \cdot \hat{I}_n}{2} \cdot cos\left(\theta_p - \delta_n - \frac{4\cdot\pi}{3}\right) + \frac{\widehat{U}_n \cdot \hat{I}_p}{2} \cdot cos\left(\theta_n - \delta_p + \frac{4\cdot\pi}{3}\right)}_{K_2} + \frac{\widehat{U}_0 \cdot \hat{I}_n}{2} \\
&\quad \cdot cos\left(\alpha_0 - \delta_n - \frac{2\cdot\pi}{3}\right) + \frac{\widehat{U}_0 \cdot \hat{I}_p}{2} \cdot cos\left(\alpha_0 - \delta_p + \frac{2\cdot\pi}{3}\right)
\end{aligned}
\tag{9.4}
$$

Using the trigonometric relation $\cos(\alpha + \beta) = \cos(\alpha) \cdot \cos(\beta) - \sin(\alpha) \cdot \sin(\beta)$ and doing simplifications, equations (9.4) becomes:

$$
\begin{aligned}
P_{imb\,L1} &= K_1 + \widehat{U}_0 \cdot cos(\alpha_0) \cdot \underbrace{\left[\frac{\hat{I}_n}{2} \cdot cos(\delta_n) + \frac{\hat{I}_p}{2} \cdot cos(\delta_p)\right]}_{K_3 = \frac{1}{2}\cdot\Re\{\underline{I}_{L_1}\}} + \widehat{U}_0 \cdot sin(\alpha_0) \\
&\quad \cdot \underbrace{\left[\frac{\hat{I}_n}{2} \cdot sin(\delta_n) + \frac{\hat{I}_p}{2} \cdot sin(\delta_p)\right]}_{K_4 = \frac{1}{2}\cdot\Im\{\underline{I}_{L_1}\}}
\end{aligned}
\tag{9.5}
$$

$$P_{imb\,L2} = K_2 + \widehat{U}_0 \cdot cos(\alpha_0) \cdot \underbrace{\left[\frac{\hat{I}_n}{2} \cdot cos\left(\delta_n + \frac{2 \cdot \pi}{3}\right) + \frac{\hat{I}_p}{2} \cdot cos\left(\delta_p - \frac{2 \cdot \pi}{3}\right)\right]}_{K_5 = \frac{1}{2} \cdot \Re\{\underline{I}_{L2}\}} +$$

$$+\widehat{U}_0 \cdot sin(\alpha_0) \cdot \underbrace{\left[\frac{\hat{I}_n}{2} \cdot sin\left(\delta_n + \frac{2 \cdot \pi}{3}\right) + \frac{\hat{I}_p}{2} \cdot sin\left(\delta_p - \frac{2 \cdot \pi}{3}\right)\right]}_{K_6 = \frac{1}{2} \cdot \Im\{\underline{I}_{L2}\}}$$

This equations can be modified to the next ones:

$$\begin{aligned} \frac{P_{imb\,L1} - K_1}{cos(\alpha_0)} &= \widehat{U}_0 \cdot K_3 + \widehat{U}_0 \cdot K_4 \cdot tan(\alpha_0) \\ \frac{P_{imb\,L2} - K_2}{cos(\alpha_0)} &= \widehat{U}_0 \cdot K_5 + \widehat{U}_0 \cdot K_6 \cdot tan(\alpha_0) \end{aligned} \tag{9.6}$$

Dividing the first one by the second one:

$$\frac{P_{imb\,L1} - K_1}{P_{imb\,L2} - K_2} = \frac{K_3 + K_4 \cdot tan(\alpha_0)}{K_5 + K_6 \cdot tan(\alpha_0)} \tag{9.7}$$

Now it is possible to isolate the $tan(\alpha_0)$ as shown in equation (9.8).

$$\tan(\alpha_0) = \frac{(P_{imb\,L2} - K_2) \cdot K_3 - (P_{imb\,L1} - K_1) \cdot K_5}{(P_{imb\,L1} - K_1) \cdot K_6 - (P_{imb\,L2} - K_2) \cdot K_4} \tag{9.8}$$

Injecting (9.8) in (9.6), the amplitude of the zero sequence voltage can be evaluated.

$$\widehat{U}_0 = \frac{P_{imb\,L1} - K_1}{K_3 \cdot cos(\alpha_0) + K_4 \cdot sin(\alpha_0)} = \frac{P_{imb\,L2} - K_2}{K_5 \cdot cos(\alpha_0) + K_6 \cdot sin(\alpha_0)} \tag{9.9}$$

The equation (9.9) shows 2 different ways to compute the amplitude of the zero sequence voltage. It is recommended to use the one that has the biggest denominator.

Note that the different variables K_1 to K_6 are define here below.

$$\begin{aligned} K_1 &= \frac{\widehat{U}_p \cdot \hat{I}_n}{2} \cdot cos(\theta_p - \delta_n) + \frac{\widehat{U}_n \cdot \hat{I}_p}{2} \cdot cos(\theta_n - \delta_p) \\ K_2 &= \frac{\widehat{U}_p \cdot \hat{I}_n}{2} \cdot cos\left(\theta_p - \delta_n - \frac{4 \cdot \pi}{3}\right) + \frac{\widehat{U}_n \cdot \hat{I}_p}{2} \cdot cos\left(\theta_n - \delta_p + \frac{4 \cdot \pi}{3}\right) \\ K_3 &= \frac{\hat{I}_n}{2} \cdot cos(\delta_n) + \frac{\hat{I}_p}{2} \cdot cos(\delta_p) \\ K_4 &= \frac{\hat{I}_n}{2} \cdot sin(\delta_n) + \frac{\hat{I}_p}{2} \cdot sin(\delta_p) \\ K_5 &= \frac{\hat{I}_n}{2} \cdot cos\left(\delta_n + \frac{2 \cdot \pi}{3}\right) + \frac{\hat{I}_p}{2} \cdot cos\left(\delta_p - \frac{2 \cdot \pi}{3}\right) \\ K_6 &= \frac{\hat{I}_n}{2} \cdot sin\left(\delta_n + \frac{2 \cdot \pi}{3}\right) + \frac{\hat{I}_p}{2} \cdot sin\left(\delta_p - \frac{2 \cdot \pi}{3}\right) \end{aligned} \tag{9.10}$$

To evaluate the different quantities in the variables K_1 to K_6, the equations (9.11) are used.

$$\hat{I}_p = \sqrt{i_d^{+2} + i_q^{+2}},\ \ \delta_p = atan2\left(\frac{i_q^+}{i_d^+}\right),\ \ \hat{I}_n = \sqrt{i_d^{-2} + i_q^{-2}},\ \ \delta_n = -\,atan2\left(\frac{i_q^-}{i_d^-}\right) \tag{9.11}$$

$$\widehat{U}_p = \sqrt{{u_d^+}^2 + {u_q^+}^2},\ \theta_p = atan2\left(\frac{u_q^+}{u_d^+}\right),\ \widehat{U}_n = \sqrt{{u_d^-}^2 + {u_q^-}^2},\ \theta_n = -\,atan2\left(\frac{u_q^-}{u_d^-}\right)$$

9.2 ZSCC DEVELOPMENT

Let assume that all the quantities are sinusoidal. The SDBC exchange positive and negative sequence currents with the grid. The grid contains positive and negative sequence voltages. Moreover the converter generates an internal zero sequence current. These definitions are shown in the equations (9.12).

$$\begin{aligned}
\underline{I}_{L_{12}} &= \hat{I}_p \cdot e^{j\cdot\delta_p} + \hat{I}_n \cdot e^{j\cdot\delta_n} + \hat{I}_0 \cdot e^{j\cdot\delta_0} \\
\underline{I}_{L_{23}} &= \hat{I}_p \cdot e^{j\cdot\left(\delta_p - \frac{2\cdot\pi}{3}\right)} + \hat{I}_n \cdot e^{j\cdot\left(\delta_n + \frac{2\cdot\pi}{3}\right)} + \hat{I}_0 \cdot e^{j\cdot\delta_0} \\
\underline{I}_{L_{31}} &= \hat{I}_p \cdot e^{j\cdot\left(\delta_p + \frac{2\cdot\pi}{3}\right)} + \hat{I}_n \cdot e^{j\cdot\left(\delta_n - \frac{2\cdot\pi}{3}\right)} + \hat{I}_0 \cdot e^{j\cdot\delta_0} \\
\underline{U}_{SML1} &= \widehat{U}_p \cdot e^{j\cdot\theta_p} + \widehat{U}_n \cdot e^{j\cdot\theta_n} \\
\underline{U}_{SML2} &= \widehat{U}_p \cdot e^{j\cdot\left(\theta_p - \frac{2\cdot\pi}{3}\right)} + \widehat{U}_n \cdot e^{j\cdot\left(\theta_n + \frac{2\cdot\pi}{3}\right)} \\
\underline{U}_{SML3} &= \widehat{U}_p \cdot e^{j\cdot\left(\theta_p + \frac{2\cdot\pi}{3}\right)} + \widehat{U}_n \cdot e^{j\cdot\left(\theta_n - \frac{2\cdot\pi}{3}\right)}
\end{aligned} \tag{9.12}$$

The active power in each phase can be calculated by:

$$P_{L_{ij}} = \Re\left\{\underline{S}_{L_{ij}}\right\} = \Re\left\{\underline{U}_{SML_i} \cdot \underline{I}^*_{L_{ij}}\right\} = P_{com} + P_{imb\,Lij} \tag{9.13}$$

with:

$$P_{com} = \frac{\widehat{U}_p \cdot \hat{I}_p}{2} \cdot cos(\theta_p - \delta_p) + \frac{\widehat{U}_n \cdot \hat{I}_n}{2} \cdot cos(\theta_n - \delta_n) = \frac{P_{3\Phi}}{3} \tag{9.14}$$

and

$$\begin{aligned}
P_{imb\,L12} &= \underbrace{\frac{\widehat{U}_p \cdot \hat{I}_n}{2} \cdot cos(\theta_p - \delta_n) + \frac{\widehat{U}_n \cdot \hat{I}_p}{2} \cdot cos(\theta_n - \delta_p)}_{K_{11}} + \frac{\widehat{U}_p \cdot \hat{I}_0}{2} \cdot cos(\theta_p - \delta_0) \\
&\quad + \frac{\widehat{U}_n \cdot \hat{I}_0}{2} \cdot cos(\theta_n - \delta_0) \\
P_{imb\,L23} &= \underbrace{\frac{\widehat{U}_p \cdot \hat{I}_n}{2} \cdot cos\left(\theta_p - \delta_n - \frac{4\cdot\pi}{3}\right) + \frac{\widehat{U}_n \cdot \hat{I}_p}{2} \cdot cos\left(\theta_n - \delta_p + \frac{4\cdot\pi}{3}\right)}_{K_2} + \frac{\widehat{U}_p \cdot \hat{I}_0}{2} \\
&\quad \cdot cos\left(\theta_p - \delta_0 - \frac{2\cdot\pi}{3}\right) + \frac{\widehat{U}_n \cdot \hat{I}_0}{2} \cdot cos\left(\theta_n - \delta_0 + \frac{2\cdot\pi}{3}\right)
\end{aligned} \tag{9.15}$$

Using the trigonometric relation $\cos(\alpha+\beta) = \cos(\alpha)\cdot\cos(\beta) - \sin(\alpha)\cdot\sin(\beta)$ and doing simplifications, equations (9.15) becomes:

$$P_{imb\,L12} = K_{11} + \hat{I}_0 \cdot cos(\delta_0) \cdot \underbrace{\left[\frac{\hat{U}_n}{2} \cdot cos(\theta_n) + \frac{\hat{U}_p}{2} \cdot cos(\theta_p)\right]}_{K_{13}=\frac{1}{2}\cdot\Re\{\underline{U}_{SML_1}\}} + \hat{I}_0 \cdot sin(\delta_0)$$

$$\cdot \underbrace{\left[\frac{\hat{U}_n}{2} \cdot sin(\theta_n) + \frac{\hat{U}_p}{2} \cdot sin(\theta_p)\right]}_{K_{14}=\frac{1}{2}\cdot\Im\{\underline{U}_{SML_1}\}}$$

$$P_{imb\,L23} = K_{12} + \hat{I}_0 \cdot cos(\delta_0) \cdot \underbrace{\left[\frac{\hat{U}_n}{2} \cdot cos\left(\theta_n + \frac{2\cdot\pi}{3}\right) + \frac{\hat{U}_p}{2} \cdot cos\left(\theta_p - \frac{2\cdot\pi}{3}\right)\right]}_{K_{15}=\frac{1}{2}\cdot\Re\{\underline{U}_{SML_2}\}} + \tag{9.16}$$

$$+\hat{I}_0 \cdot sin(\delta_0) \cdot \underbrace{\left[\frac{\hat{U}_n}{2} \cdot sin\left(\theta_n + \frac{2\cdot\pi}{3}\right) + \frac{\hat{U}_p}{2} \cdot sin\left(\theta_p - \frac{2\cdot\pi}{3}\right)\right]}_{K_{16}=\frac{1}{2}\cdot\Im\{\underline{U}_{SML_2}\}}$$

This equations can be modified to the next ones:

$$\frac{P_{imb\,L12} - K_{11}}{cos(\delta_0)} = \hat{I}_0 \cdot K_{13} + \hat{I}_0 \cdot K_{14} \cdot tan(\delta_0)$$
$$\frac{P_{imb\,L23} - K_{12}}{cos(\delta_0)} = \hat{I}_0 \cdot K_{15} + \hat{I}_0 \cdot K_{16} \cdot tan(\delta_0) \tag{9.17}$$

Dividing the first one by the second one:

$$\frac{P_{imb\,L12} - K_{11}}{P_{imb\,L23} - K_{12}} = \frac{K_{13} + K_{14} \cdot tan(\delta_0)}{K_{15} + K_{16} \cdot tan(\delta_0)} \tag{9.18}$$

Now it is possible to isolate the $tan(\alpha_0)$ as shown in equation (9.19).

$$tan(\delta_0) = \frac{(P_{imb\,L23} - K_{12}) \cdot K_{13} - (P_{imb\,L12} - K_{11}) \cdot K_{15}}{(P_{imb\,L12} - K_{11}) \cdot K_{16} - (P_{imb\,L23} - K_{12}) \cdot K_{14}} \tag{9.19}$$

Injecting (9.19) in (9.17), the amplitude of the zero sequence current can be evaluated.

$$\hat{I}_0 = \frac{P_{imb\,L12} - K_{11}}{K_{13} \cdot cos(\delta_0) + K_{14} \cdot sin(\delta_0)} = \frac{P_{imb\,L23} - K_{12}}{K_{15} \cdot cos(\delta_0) + K_{16} \cdot sin(\delta_0)} \tag{9.20}$$

The equation (9.20) shows 2 different ways to compute the amplitude of the zero sequence current. It is recommended to use the one that has the biggest denominator.

Note that the different variables K_{11} to K_{16} are define here below.

$$K_{11} = \frac{\hat{U}_p \cdot \hat{I}_n}{2} \cdot cos(\theta_p - \delta_n) + \frac{\hat{U}_n \cdot \hat{I}_p}{2} \cdot cos(\theta_n - \delta_p)$$
$$K_{12} = \frac{\hat{U}_p \cdot \hat{I}_n}{2} \cdot cos\left(\theta_p - \delta_n - \frac{4\cdot\pi}{3}\right) + \frac{\hat{U}_n \cdot \hat{I}_p}{2} \cdot cos\left(\theta_n - \delta_p + \frac{4\cdot\pi}{3}\right)$$
$$K_{13} = \frac{\hat{U}_n}{2} \cdot cos(\theta_n) + \frac{\hat{U}_p}{2} \cdot cos(\theta_p) \tag{9.21}$$
$$K_{14} = \frac{\hat{U}_n}{2} \cdot sin(\theta_n) + \frac{\hat{U}_p}{2} \cdot sin(\theta_p)$$
$$K_{15} = \frac{\hat{U}_n}{2} \cdot cos\left(\theta_n + \frac{2\cdot\pi}{3}\right) + \frac{\hat{U}_p}{2} \cdot cos\left(\theta_p - \frac{2\cdot\pi}{3}\right)$$

$$K_{16} = \frac{\widehat{U}_n}{2} \cdot sin\left(\theta_n + \frac{2 \cdot \pi}{3}\right) + \frac{\widehat{U}_p}{2} \cdot sin\left(\theta_p - \frac{2 \cdot \pi}{3}\right)$$